CHAPTER III

RESULT AND DISCUSSION

Chitin-chitosan exhibits high crystallinity through inter- and intramolecular hydrogen bond network. Thus, the compound possesses poor solubility. In order to overcome the poor solubility of chitosan in organic solvents, chemical modification of chitosan has been carried out. The following scheme shows all the chemical modifications done to the chitosan. The obtained products were also induced into nanospheres.

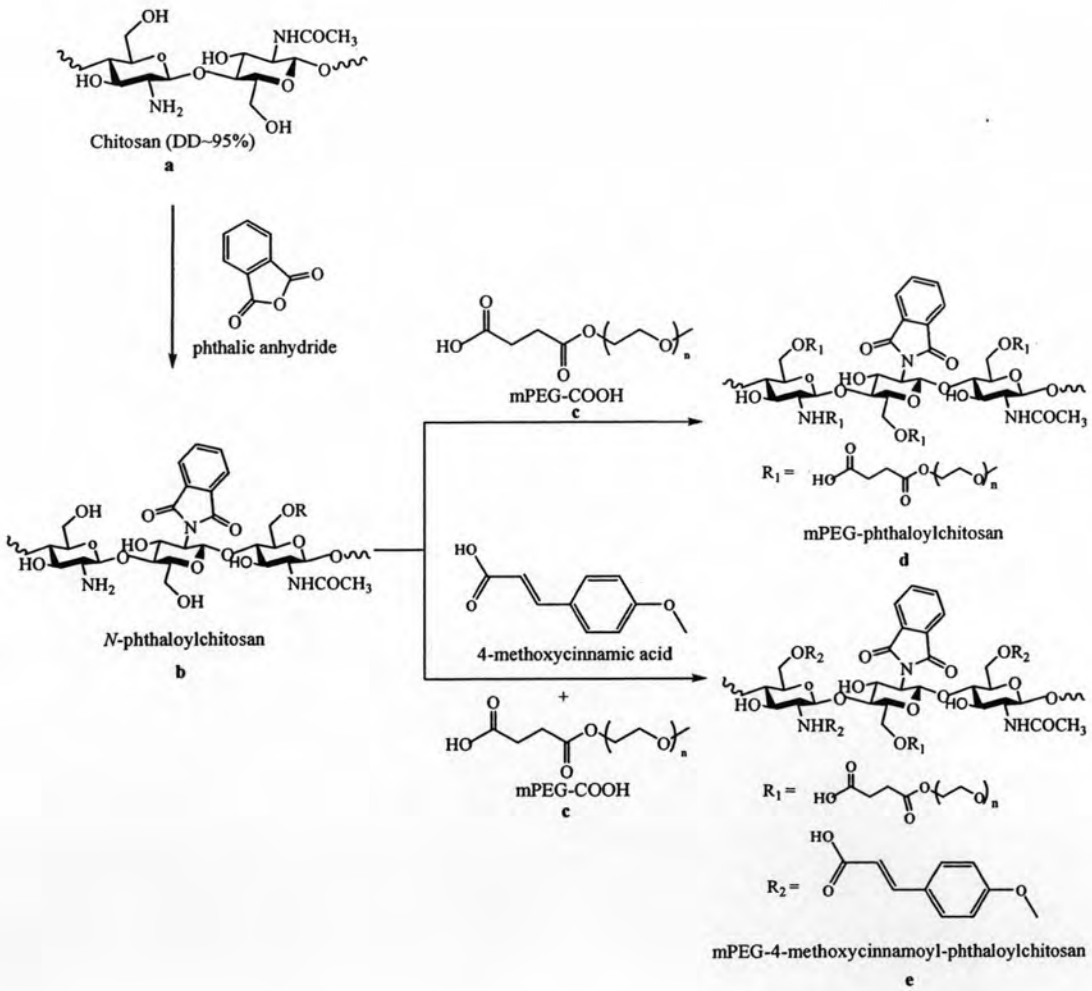

Scheme 3.1

A. Synthesis of nanoparticles

3.1 mPEG-phthaloylchitosan Nanoparticles

3.1.1 *N*-phthaloylchitosan (**b**)

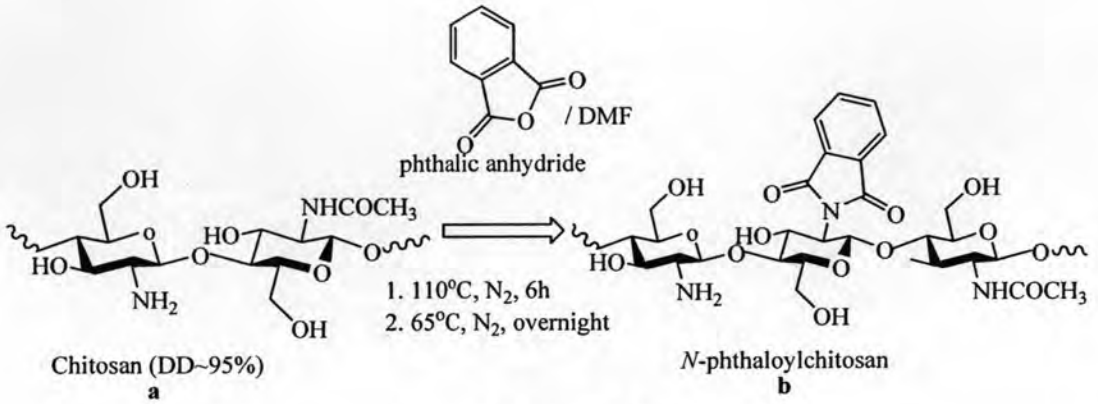

Scheme 3.2

When phthalic anhydride (13.623 g, 5-fold excess) were added into chitosan solution (3 g of chitosan in 20 mL DMF). The mixture was heated at 110°C under nitrogen for 6 hour. The temperature was reduced to 65°C and the mixture was left for 12 h. After 12 h, the mixture was filtered to separate remaining undissolved chitosan. Chitosan chains with enough phthalimido-moieties could be dissolved in DMF while those with none or too little phthalimido-moieties remained undissolved. The reason that phthaloylation could not take place in some chitosan sections may be a result of inhomogeneous deacetylation reaction of chitin into chitosan. The remaining undissolved chitosan in the reaction mixture probably was chitosan with very low % deacetylation.

When the phthaloylchitosan solution was poured into ice water, pale yellow precipitate was observed. DMF was washed out from the precipitate with excess water. The precipitate was collected, washed with excess methanol and dried to obtain 5 g (95% yields) of the product. IR spectrum (KBr) of the product confirmed successful phthaloylation onto chitosan: new peaks of the phthalimido group at 1778 and 1710 cm^{-1} referring to carbonyl anhydride and 721 cm^{-1} belonging to aromatic ring (see Figure 3.1). In addition, ^{1}H-NMR also supported the successful phthloylation (the presence of peak at 7.6-7.9 ppm belonging to protons of the phenyl ring, see Figure 3.2).

From these results, it was concluded that the phthalimido group was successfully introduced onto chitosan. The product can be dissolved in DMF and DMSO (the starting chitosan was insoluble in both solvents). This solubility had made it possible for other chemical modification on the polymer chain.

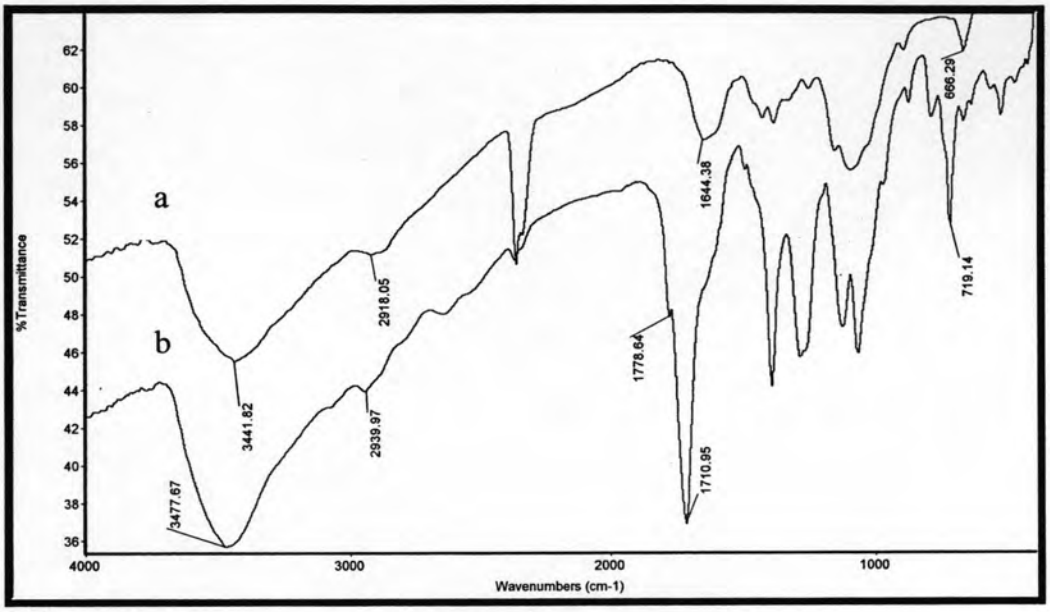

Figure 3.1 IR spectra (KBr) of a) Chitosan (compound **a**)
b) *N*-phthaloylchitosan (compound **b**)

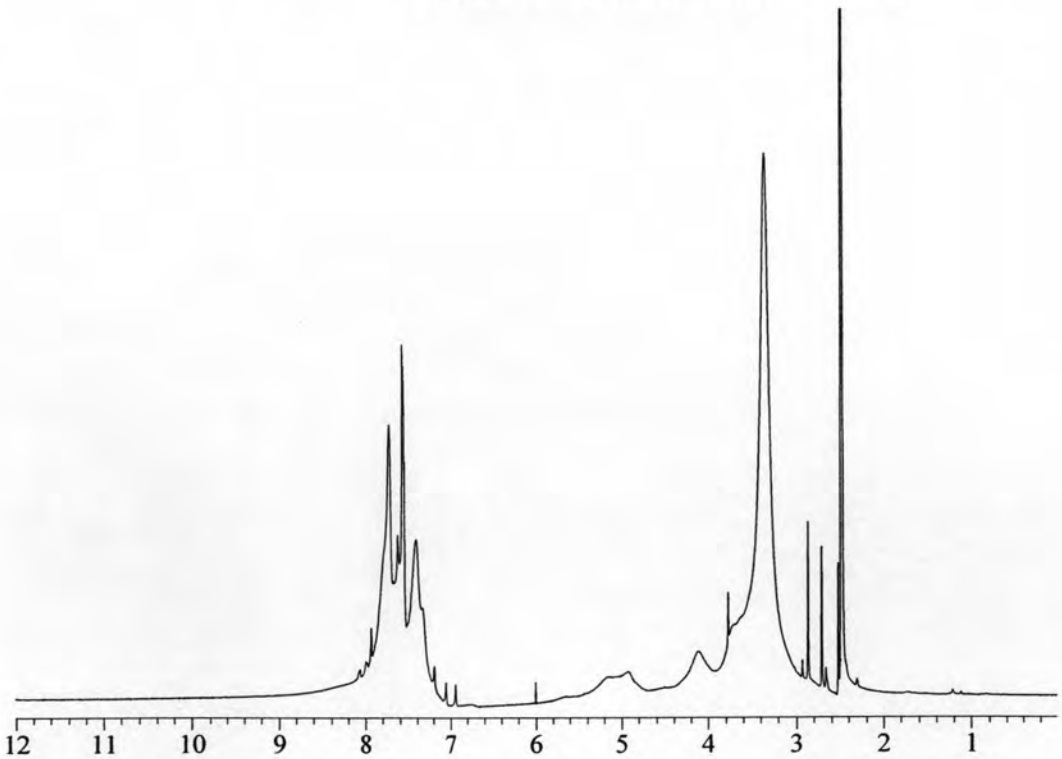

Figure 3.2 ^{1}H-NMR spectrum of *N*-phthaloylchitosan (compound **b**) (DMSO deuterated)

The substitution percentage of the phthaloyl group on chitosan backbone was estimated from the ^{1}H-NMR to be 121.95%. In short, integration at 6.8-8.2 ppm represented 4H from phthaloyl moiety while integration from 3.0-5.8 ppm representied 7H from the pyranose ring. Interference from HOD peak at 3.3 ppm (in DMSO-d_6) could be substrated out using information from spectrum of the DMSO-d_6. This was done by determining the ratio of the HOD peak area (at 3.3 ppm) and DMSO peak area (at 2.5 ppm) from the solvent spectrum. Then the HOD peak area in the phthaloylchitosan spectrum was calculated based on the peak area of the DMSO peak (at 2.5 ppm) using the obtained ratio. It should be noted here that care was taken during the preparation of samples for ^{1}H-NMR; same DMSO-d_6 solvent was used in all samples and samples were carefully dried just prior to the sample preparation. Thus the peaks area at 3.0-5.8 ppm representing 7H from the pyranose ring could be obtained by substrating out the calculated HOD peak area.

The %substitution of > 100% indicated that phthaloyl group was put not only on the amino functionality, but also on some hydroxyl groups. As a result, some crosslinking may occur. It should be noted here that ^{1}H-NMR spectrum indicated less than 0.2% N-Ac on the chitosan (almost unnoticeable resonance of N-Ac protons at 2.0 ppm). The general spectrum of the *N*-phthaloylcihtosan is shown below.

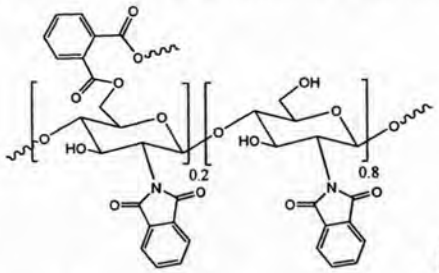

M.W. 203,005

3.1.2 Preparation of Poly (ethylene glycol) methyl ether terminated with Carboxylic Groups (**c**)

When poly(ethylene glycol) methyl ether (mPEG 3 g) was reacted with succinic anhydride 0.06 g (1 mole equiv to mPEG) in 2 mL DMF at 60°C for 17 h with a catalytic amount of pyridine. After 17 h, the solution mixture was extracted by diethyl ether and dried to give white powder of mPEG-COOH, **c**. Compound **c** shows peaks at 2888 cm^{-1} belonging to methylene group, 1736 cm^{-1} for carbonyl, and 1111 cm^{-1} for ether bond (C-O-C) (see Figure 3.3). ^{1}H-NMR also confirmed the successful of the reaction as seen from new peak at 2.8 ppm possessing to methylene protons in succinic anhydride (see in Figure 3.4).

From these results, it was concluded that the hydroxyl group at the terminal of mPEG has been replaced with succinyl moeity.

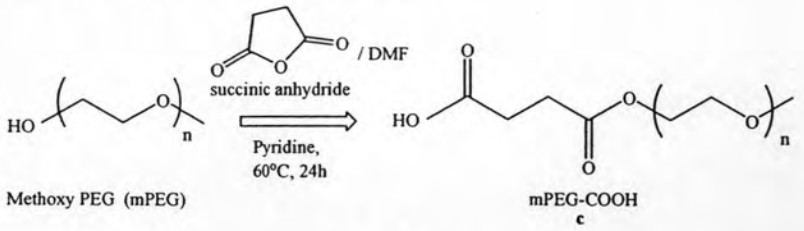

Scheme 3.3

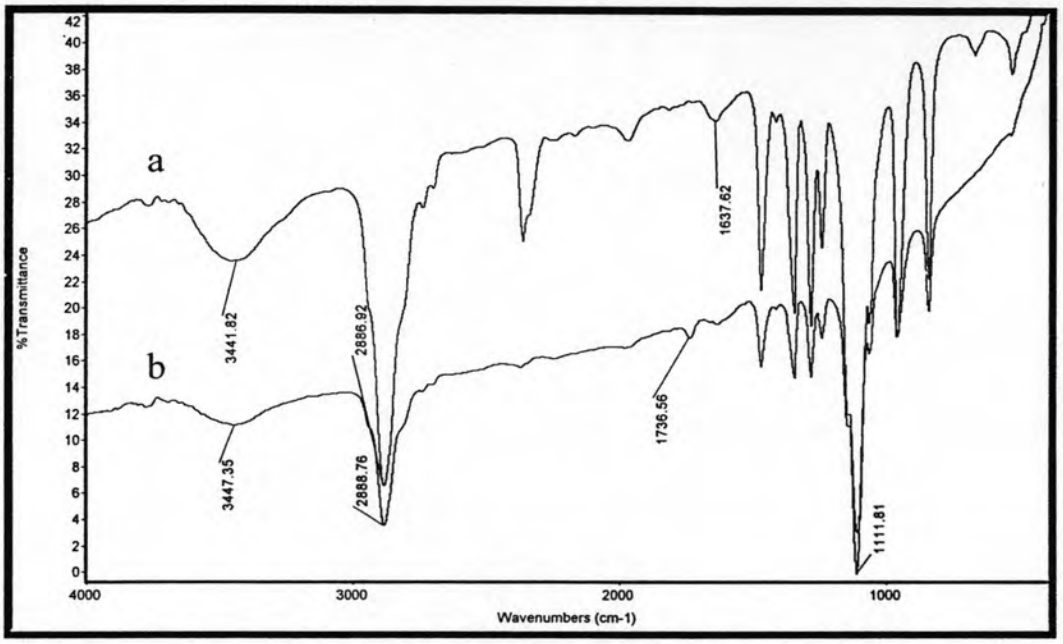

Figure 3.3 IR spectra (KBr) of a) mPEG b) mPEG-COOH (compound **c**)

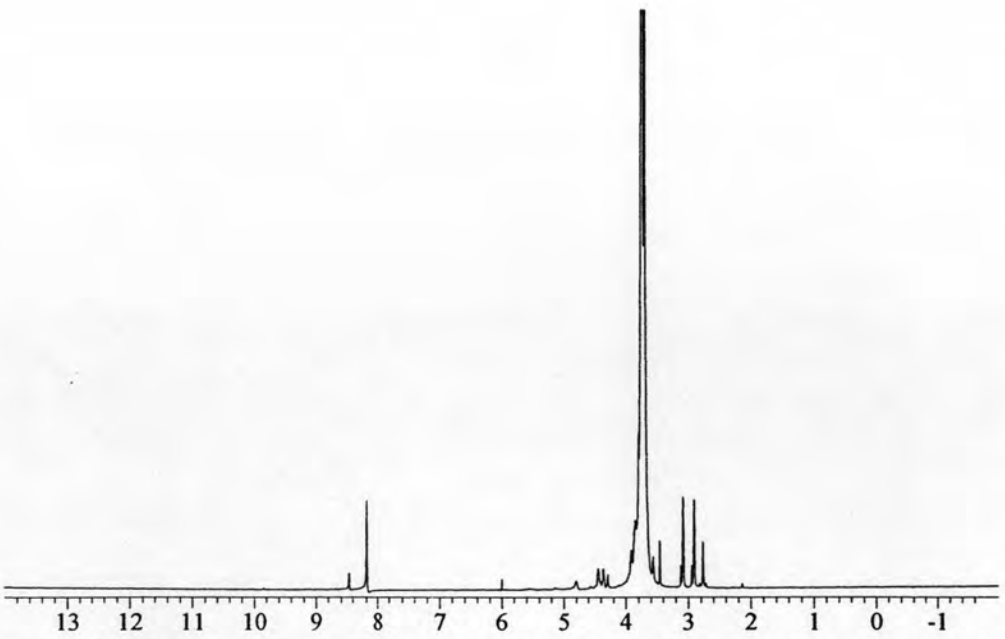

Figure 3.4 ^{1}H-NMR spectrum of mPEG-COOH (compound **c**) (DMF deuterated)

3.1.3 mPEG-phthaloylchitosan Nanoparticles (**d**)

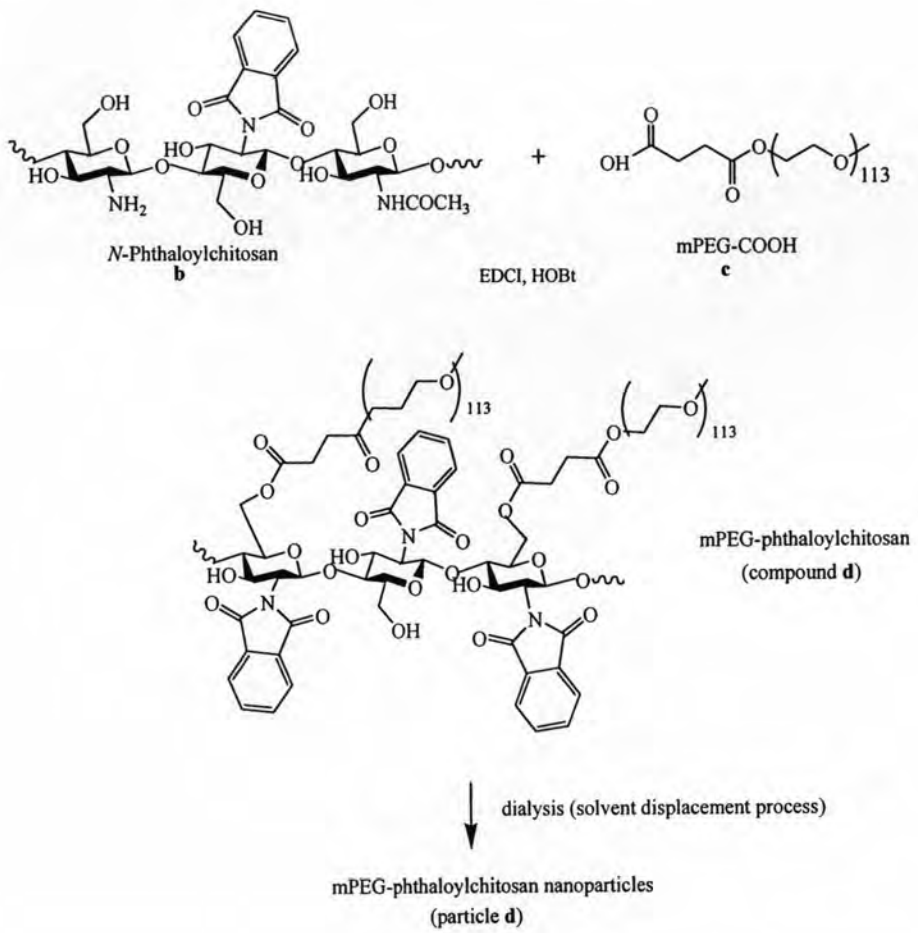

Scheme 3.4

Compound **c** (7.57 g, 0.4 mol equivalents to hydroxyl group in phthaloylchitosan) was stirred with compound **b** (1 g in 20 mL of DMF) containing HOBt (0.602g, 3 mol equivalents to compound **c**) at room temperature until the solution was clear. EDCI (0.8535 g, 3 mol equivalents to compound **c**) was added to react at 4°C for 30 min and then room temperature for 12 h. The mixture was dialyzed in water for 5 days (1,000×15 mL change of water) before thoroughly washed with methanol and dried to obtain white particles, **d**. FTIR (KBr, cm^{-1}): 3477 (OH), 2882 (C-H stretching), 1778 and 1710 (C=O anhydride), 1710 (C=O ester), and 721 (aromatic ring). ^{1}H-NMR (DMF-d_7, δ, ppm): 2.0 (s, $NCOCH_3$), 2.7 (s, $-OCCH_2CH_2CO-$), 3.4 (s, OCH_3 of PEG), 3.8 (b, $-OCH_2CH_2O-$ of PEG), 3.6-6.0 ($-OCH_2CH_2O$ of PEG and H1-H6 of glucosamine), and 7.6-8.0 (aromatic ring) (see Figure 3.6).

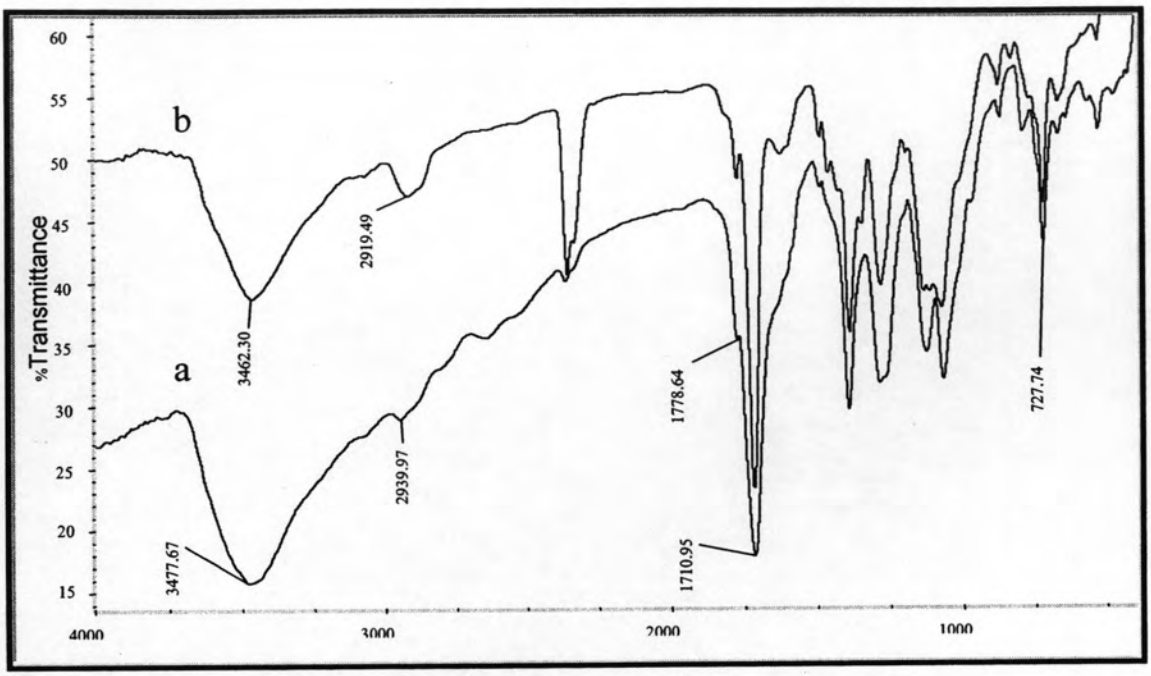

Figure 3.5 IR spectra (KBr) of a) *N*-phthaloylchitosan (compound **b**)
b) mPEG-phthaloylchitosan nanoparticles (Particle **d**)

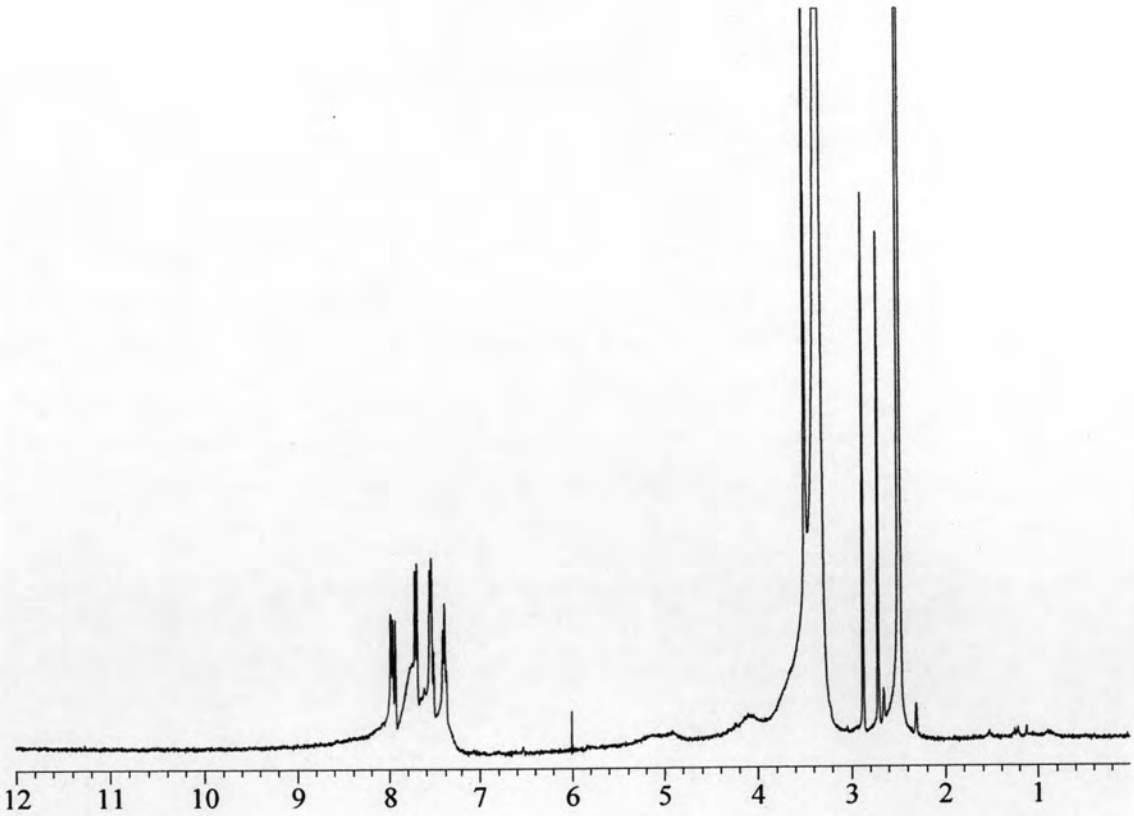

Figure 3.6 ^{1}H-NMR spectrum of mPEG-phthaloylchitosan nanoparticles (Particle **d**) (DMSO deuterated)

Furthermore, experiments were done to obtain UV absorption properties (λ_{max}, ε) of this product. As shown in Figure 3.7, the product gave two new absorption bands, λ_{max} of 331 nm and 346 nm in DMSO. After grafting mPEG-COOH onto compound **b,** the product with UVA absorption property was obtained.

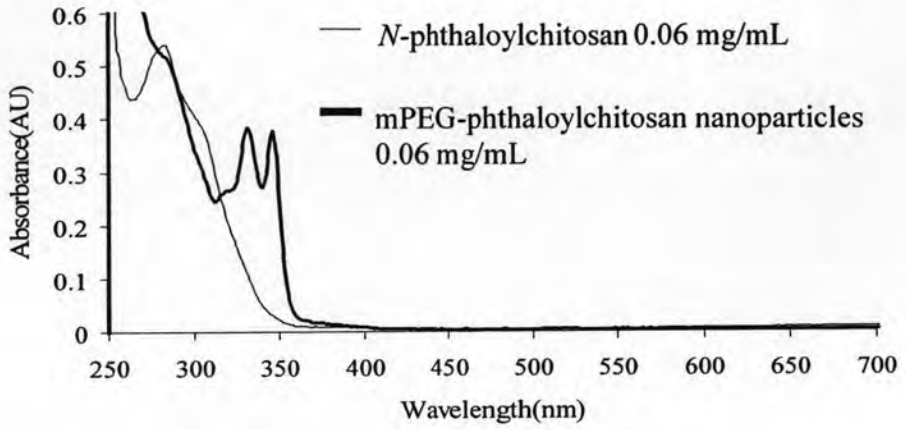

Figure 3.7 UV absorption spectra of mPEG-phthaloylchitosan nanoparticles (0.06 mg/mL in DMSO)

Substitution percentage of PEG on the phthaloylchitosan could be obtained from ^{1}H-NMR spectrum. This was done by using the peak area at 6.8-8.2 ppm which represented phthaloyl moieties, and the peaks area at 3-5.8 ppm which represented 7H from each pyranose ring of chitosan and 452H from each PEG unit. The interference from HOD peak at 3.3 ppm was substrated out using the same method as described previously for determining the %substitution of phthaloyl moieties (p.38). Since the %substitution of phthaloyl moieties was known, calculation of peak area representing 7H of pyranose ring could be achieved using information of 6.8-8.2 ppm peak area. Thus the peak area representing PEG could be calculated. Calculation gave %substitution of PEG = 7%. General structure of the product is as followed:

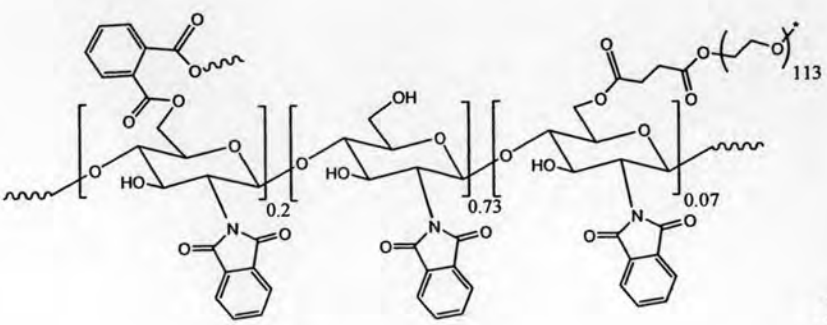

M.W. 428,402

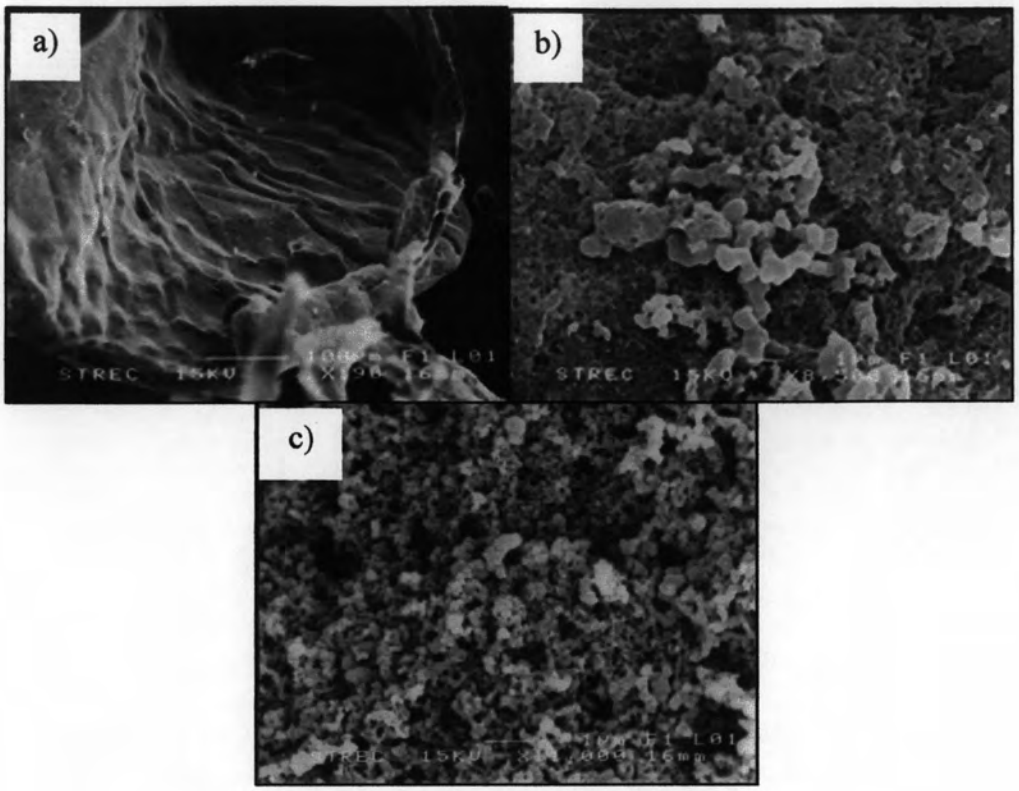

Figure 3.8 SEM photographs at 14 kV of a) Chitosan (×190) b) *N*-phthaloylchitosan (×8,500) c) mPEG-phthaloylchitosan nanoparticles (×8,500)

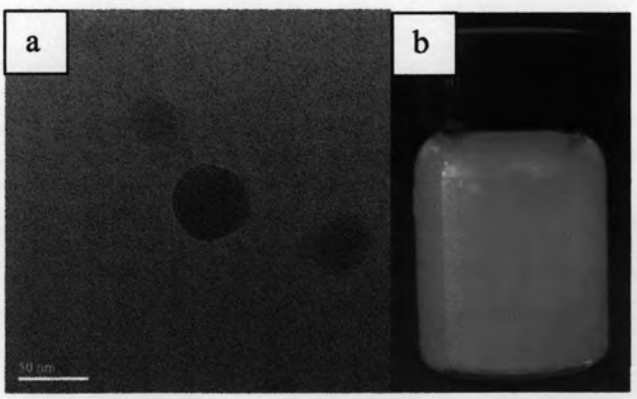

Figure 3.9 a) TEM photographs of mPEG-phthaloylchitosan nanoparticles (×8,000)
b) Colloidal solution of mPEG-phthaloylchitosan (particle **d**) (3 g/L in water)

Formation of nanoparticles and the effect of solvent

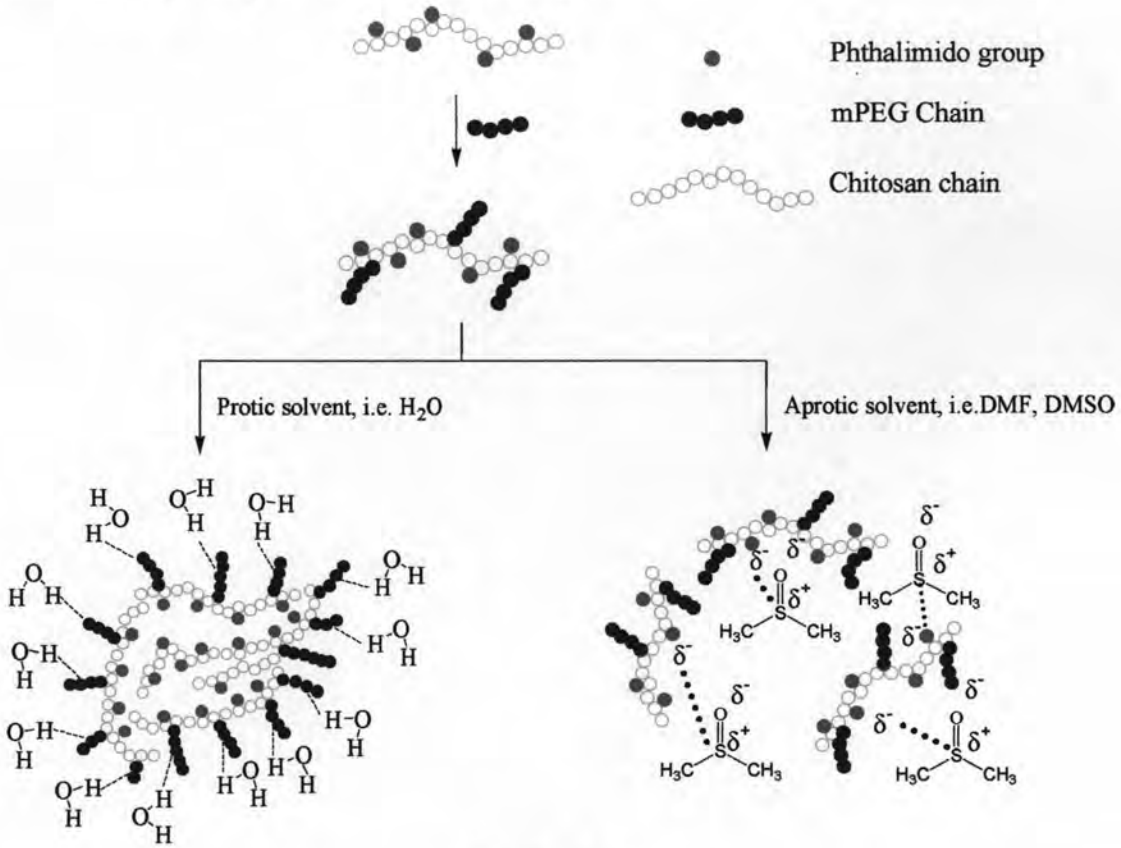

Scheme 3.5

As mentioned above, it was found that chitosan showed irregular non-nano structure (Figure 3.8 (**a**)), while N-phthaloylchitosan gives partially round shape (Figure 3.8 (**b**)) and mPEG-phthaloylchitosan particles showed nanospheric structure (Figure 3.8 (**c**)), respectively. The appearance of N-phthaloylchitosan implies an initial step of sphere formation as a result of phthalimido groups in chitosan chain. The chitosan-nanoparticle obtained from grafting mPEG-COOH with M_n = 5,100 Dalton show the average sizes in the range of 40-150 nm as declared by TEM (Figure 3.9) and SEM (Figure 3.8). Well-defined spheres existed in the colloidal aqueous solution as shown in Figure 3.9. Better dispersion of mPEG-phthaloylchitosan nanoparticles over phthaloylchitosan nanoparticles might come from the fact that there are some hydrations by hydrogen bonds between water and mPEG-phthaloylchitosan nanoparticles (at oxygen atoms of mPEG on chitosan chain) (Scheme 5). In addition, concentration of mPEG-phthaloylchitosan during dialysis process affects the size of the obtained particles. Dialysis at lower concentration of mPEG-phthaloylchitosan gave smaller sphere comparing to the product obtained from

dialysis at higher concentrations (Figure 3.10). The result of the zeta potential indicates a marked negative charge of the mPEG-phthaloylchitosan (-30.3 mV). Average particle size distribution of the particles is 255 nm.

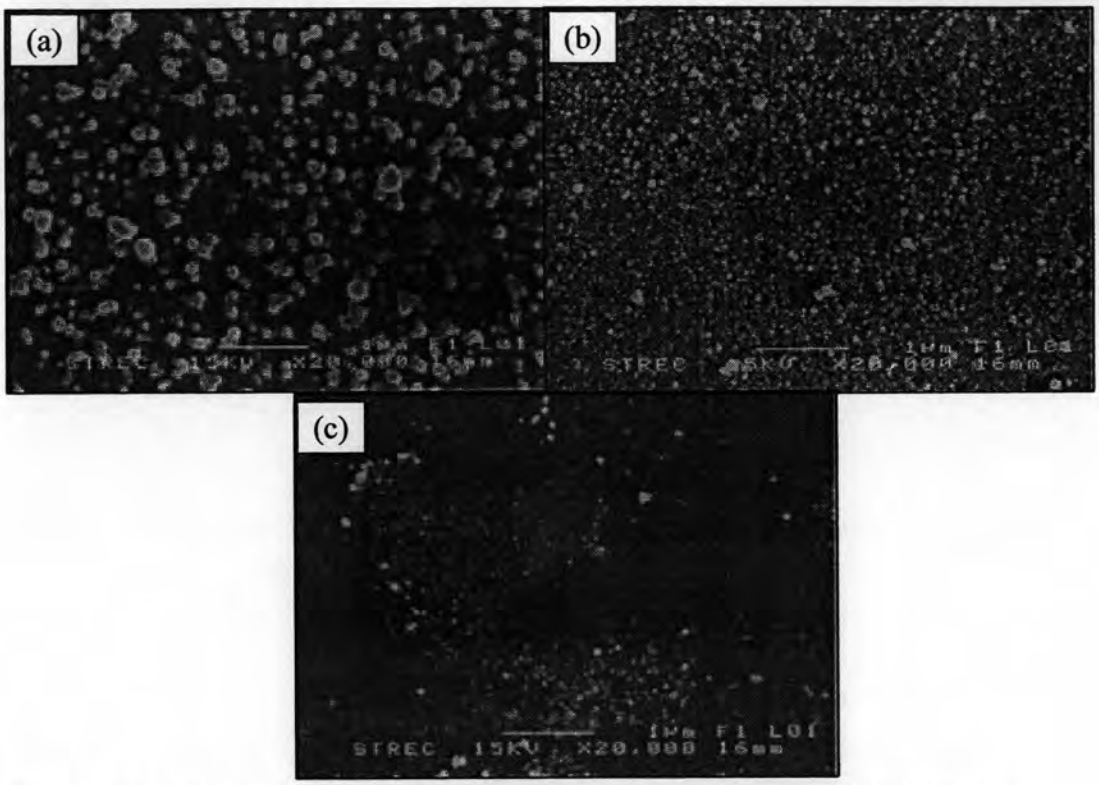

Figure 3.10 Dialyses at various concentration of nanoparticle **d** (a) 30,000 ppm (b) 3,000 ppm (c) 300 ppm (×20,000)

Anti-microbial study of aqueous mPEG-phthaloylchitosan-nanoparticles dispersion using *Staphylococcus aureus* ATCC 25923 and *Escherichia coli* ATCC 25922 bacteria, indicates that the mPEG-phthaloylchitosan nanoparticles can halt the growth of both bacteria when used at concentration of at least 625 ppm for *Staphylococcus aureus* ATCC 25923 bacteria and 5000 ppm for *Escherichia coli* ATCC 25922 bacteria. The nanoparticles, however, are not bacteriocidal.

Patch test (PT) and photopatch test (PTT) were selected as irritation tests for mPEG-phthaloylchitosan nanoparticles with UV absorption property. The results of patch testing (PT) and photopatch testing (PTT) of mPEG-phthaloylchitosan nanoparticles on forty volunteers indicated that the compound cannot trigger irritation on human skin.

After successful preparation and characterization of particle **d**, various cosmetic actives including 2-ethylhexyl-p-methoxycinnamate, ascorbyl palmitate and astaxanthin have been encapsulated into the prepared particles.

3.1.4 Encapsulated of EHMC into Particle **d**

Trans-EHMC represents the most widely used sunscreen compound, however, several studies have demonstrated that *trans*-EHMC is unstable following irradiation both in solution and in emulsion formulations [64]. To solve the problem, in this work, encapsulation of *trans*-EHMC into nanoparticle **d** was carried out.

Encapsulation was done through 1) solvent displacement technique in which the EHMC and chitosan were dissolved in DMF and then DMF was then displaced by water and 2) diffusion method in which EHMC was added into aqueous suspension of nanoparticle **d** and stirring was maintained over a period of time to allow diffusion of EHMC into the particles.

In the solvent displacement method, study was carried out to investigate the effects of displacing medium on the encapsulation efficiency (EE). The results indicated that pure water gave the maximum EE value. This was judged from UV absorption spectrum of the obtained particles (Figure 3.11). Absorption band at λ_{max} of 310 nm represents EHMC.

Dialysis against various H_2O: EtOH ratio

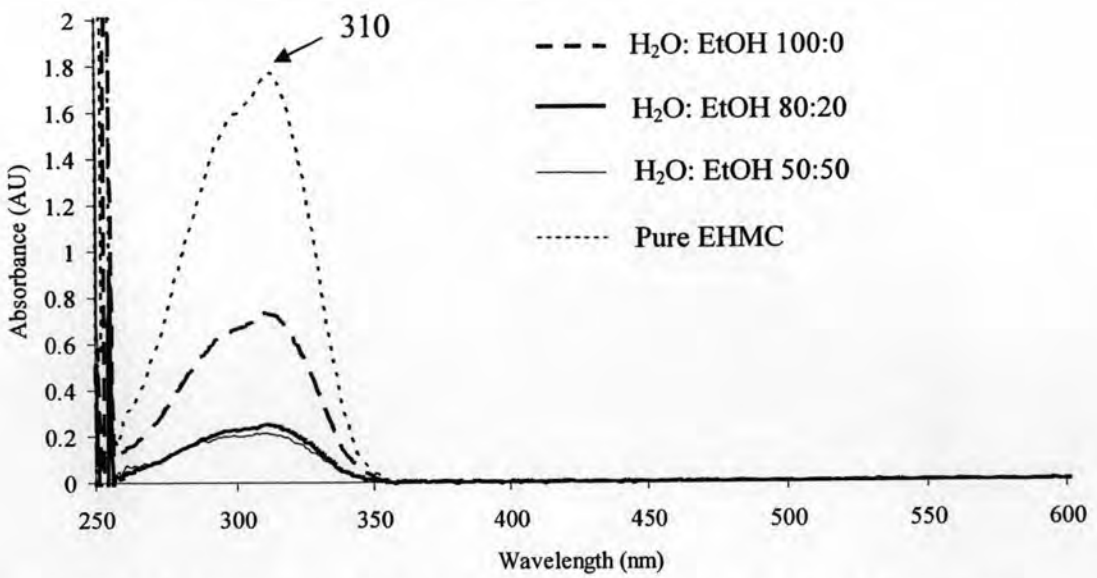

Figure 3.11 UV absorption spectra of EHMC-loaded-particle **d** (0.12 mg/ml in DMSO) and compare with pure EHMC 20 ppm

Figure 3.12 SEM photographs at 15 kV of EHMC-loaded-particle **d** (left to right: dialysis in ethanol and water, respectively) (×8,500)

Therefore, encapsulation of EHMC into nanoparticles **d** by using pure water compared with unencapsulated nanoparticles was carried out.

As can be seen in the TEM photographs (Figure 3.13), after EHMC encapsulation by solvent displacement method, the appearance of particle's border is very apparent. The size of the particle size also increases upon encapsulation. Successful encapsulation of EHMC into particle **d** was confirmed through the UV absorption spectra (Figure 3.14). The particle **d** with and without EHMC entrapment showed significant difference in UV absorption. It is obvious that an increased absorption at 310 nm of the EHMC-loaded-particle in the spectrum must be caused by the presence of EHMC. The average sizes were observed to be 150 nm as determined by SEM (Figure 3.16). With the condition used, about 97.65% (w/w) EHMC could be encapsulated into the particle. The obtained EHMC-loaded-particle contains 45 % (w/w) EHMC (Table 2) (see Appendix A for calculation).

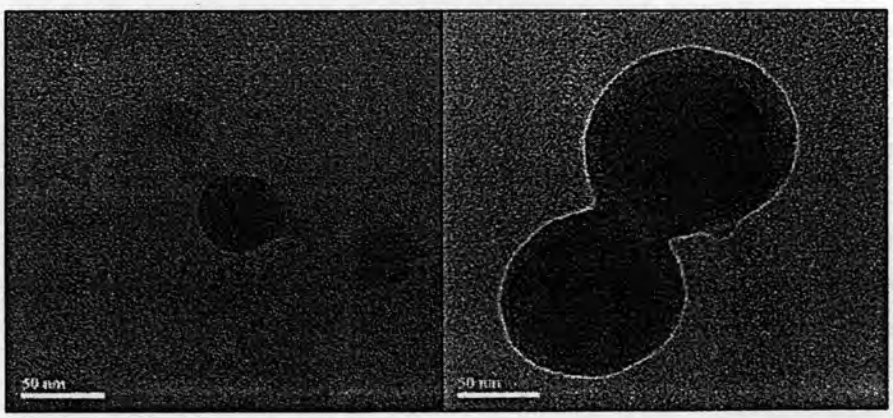

Figure 3.13 TEM photographs of particle **d** before (left) (×80,000) and after (right) EHMC encapsulation (×80,000)

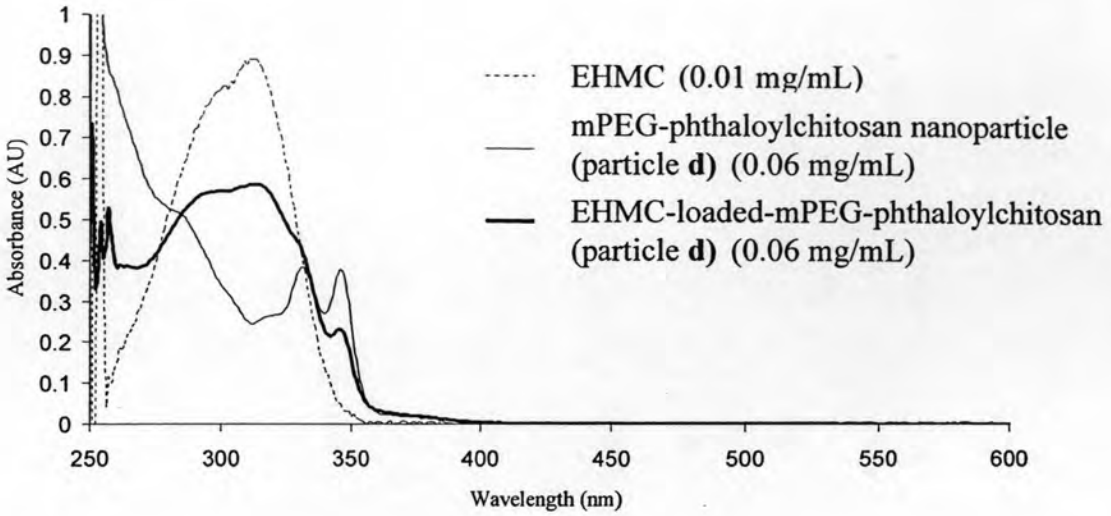

Figure 3.14 UV absorption spectra of EHMC-loaded-particle **d** (0.02 mg/ ml in DMSO)

Furthermore, study the diffusion method was carried out to investigate the effects of diffusion of EHMC into the particle on the diffusion efficiency. The results indicated that % encapsulation increased as the diffusion time increased. This was judged from UV absorption spectrum of the obtained particles (Figure 3.15). Absorption band at λ_{max} of 310 nm represents EHMC.

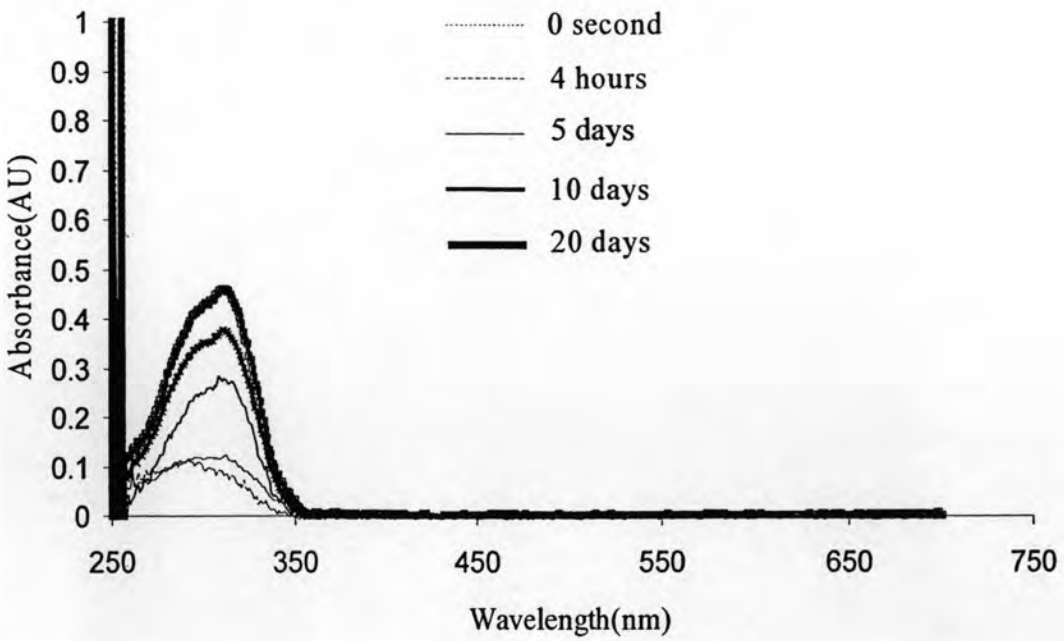

Figure 3.15 UV absorption spectra of diffusion of EHMC into particle **d** at each time (0 sec., 4 hours, 5 days, 10 days and 20 days, respectively) (0.10 mg/ ml in DMSO)

Table 1 % Diffusion efficiency and % Weight of EHMC in the particle **d** (%w/w)

Process	Time				
	0 second	4 hour	10 day	20 day	30 day
% Diffusion efficiency*	0.65	0.82	1.84	2.37	2.87
Weight of EHMC in the particle **d**** (%w/w)	1.28	1.62	2.81	4.54	5.45

*, ** see APPENDIX A for calculation

The results indicated that the encapsulation efficiency of EHMC by solvent displacement method as shown in Table 3 is better than the diffusion efficiency as mentioned above (Table 1).

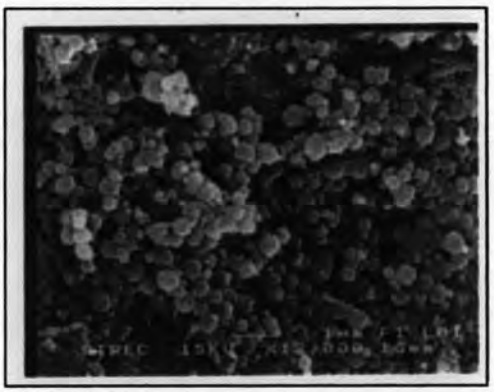

Figure 3.16 SEM photographs at 15 kV of EHMC-loaded-particle **d** (×12,000)

EHMC–loaded-particle **d** was subjected to the investigation on the release of the loaded EHMC from the nanoparticles. The test indicated the controlled release of the EHMC from the nanoparticles. The release could occur on baby mouse skin without additional need of pH or temperature induction.

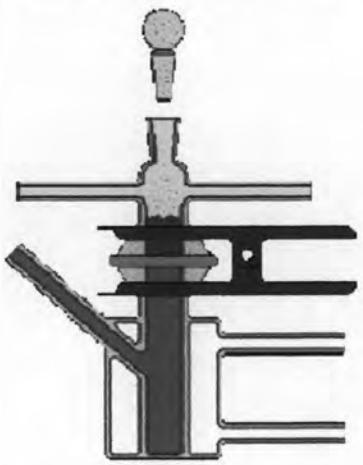

Figure 3.17 Franz-type glass diffusion cells

*Photostability test; EHMC-loaded-particle **d** and free EHMC*

Photostability is the most important characteristic of effective sunscreens. In fact the possible sunfilter photochemical decomposition reduces photoprotective properties and could also produce phototoxic and photoallergenic degradation products. It is well known that 2-ethylhexyl-p-methoxycinnamate (EHMC), UVB filter, will undergo *trans* to *cis* photoisomerization under UV light exposure resulting in the decrease in UV absorption efficiency. This configurational change will decrease the UV absorption efficiency of EHMC because the *cis* configuration possess ε of 12000 $M^{-1}cm^{-1}$ while the *trans* configuration possess ε of about 23000 $M^{-1}cm^{-1}$ [96]. To evaluate the ability of the particles **d** in shielding UV light from the loaded material, photostability of the loaded EHMC was compared with that of free EHMC at the same concentration.

Trans to *cis* photoisomerization of EHMC was monitored through ^{1}H-NMR using the integration of the *trans* EHMC proton (6.3 ppm, d, J = 16 Hz, -CH=C**H**COO-) against that of the *cis* (5.8 ppm, d, J = 12 Hz, -CH=C**H**COO-). The result indicated that the loaded EHMC was more photostable than the free EHMC (Table 2).

Table 2 Percentages of *trans* and *cis* configulation in the irradiated encapsulated-EHMC and free EHMC

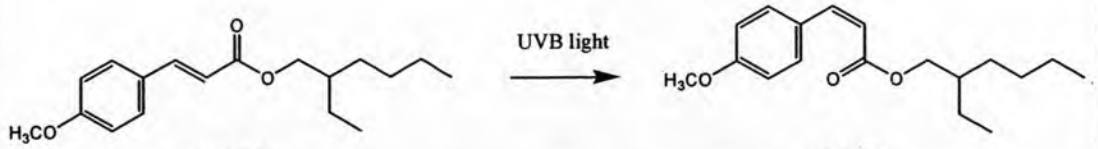

trans-OMC *cis*-OMC

UVB exposure (mJ)	% cis configuration	
	EHMC encapsulated particles	Free EHMC + unencapsulated particles
0	0	0
22.5	13	26
45	17	45

3.1.5 Encapsulation of Ascorbyl Palmitate into Particle **d**

Ascorbyl palmitate is derivative of ascorbic acid. It is a strong antioxidant. The compound can efficiently protect biological molecules against oxidative degradation. However, its low stability is a serious limitation. The compound is easily oxidized, especially under aerobic conditions, and light exposure [66]. Thus encapsulation should help increasing the stability of the compound.

Encapsulation of ascorbyl palmitate into nanoparticle **d** by solvent displacement method was carried out.

Since ascorbyl palmitate has no obvious well seperated UV-visible absorption band when compared to UV absorption spectrum of particle **d**, NMR spectroscopy was used for the analyses of ascorbyl palmitate loaded particle **d.** After encapsulation process, the washed particles were dissolved in ethanol and subjected to NMR analyzes. Presences of ^{1}H resonances at 0.8 and 1.4 ppm (representing palmitoyl moieties in ascorbyl palmitate, Figure 3.18) confirm a successful encapsulation of this vitamin C derivative into particle **d.** TEM photographs (Figure 3.19), after ascorbyl palmitate encapsulation the appearance of particle's border is very apparent. Encapsulation shows obvious size changes. The average sizes of the ascorbyl palmitate-loaded-particle **d** were observed to be 250-750 nm (diameter) as determined by SEM (Figure 3.20). The encapsulated particles appeared well dispersed in water (Figure 3.25). With the condition used, about 100% (w/w) EHMC could be encapsulated into the particle. The obtained ascorbyl palmitate-loaded-capsule contains 93.56% (w/w) ascorbyl palmitate (Table 3) (see in Appendix A for calculation).

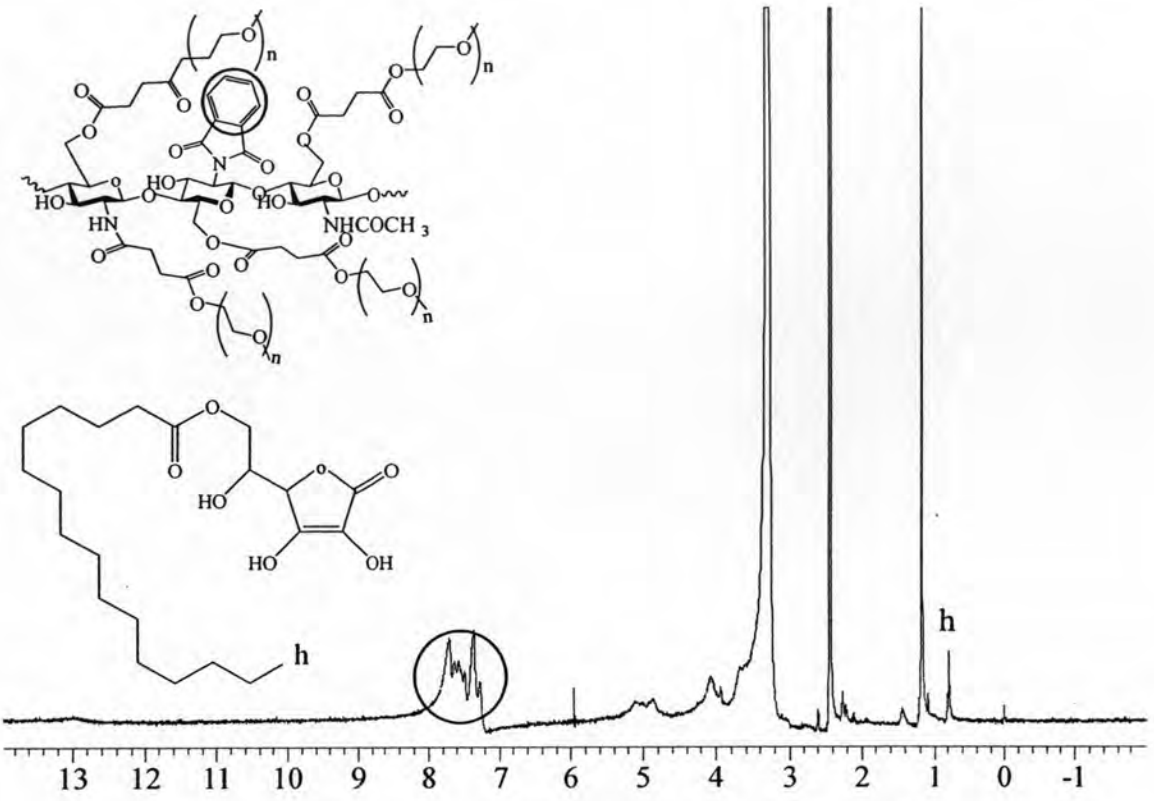

Figure 3.18 ^{1}H-NMR spectrum of ascorbyl palmitate-loaded-particle **d** (DMSO deuterated)

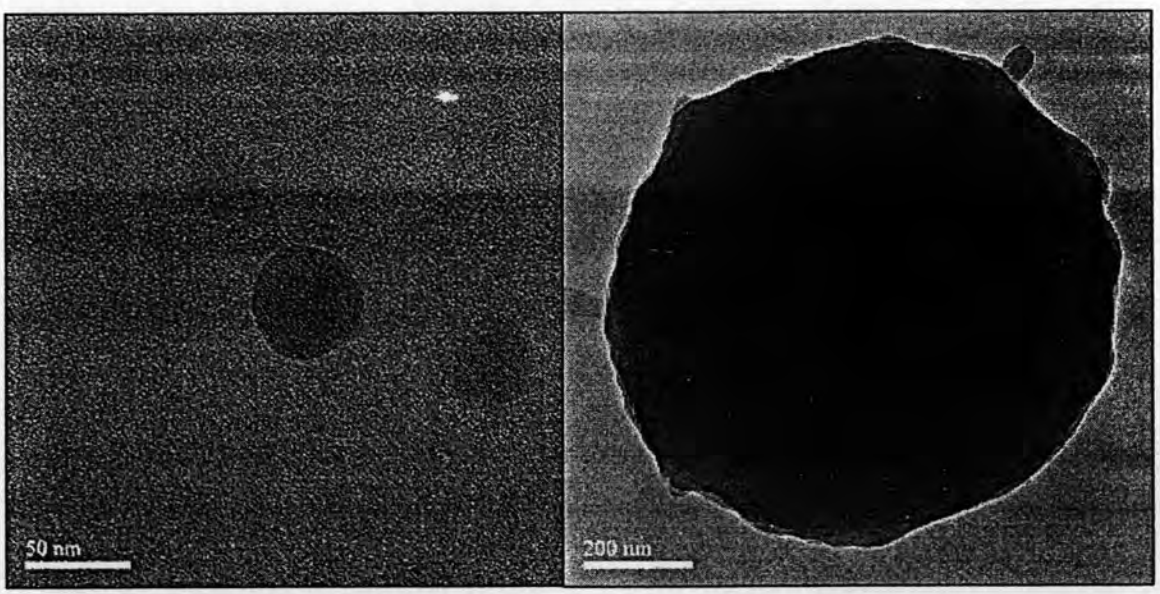

Figure 3.19 TEM photographs of particle **d** before (left) (×80,000) and after (right) ascorbyl palmitate encapsulation (×20,000)

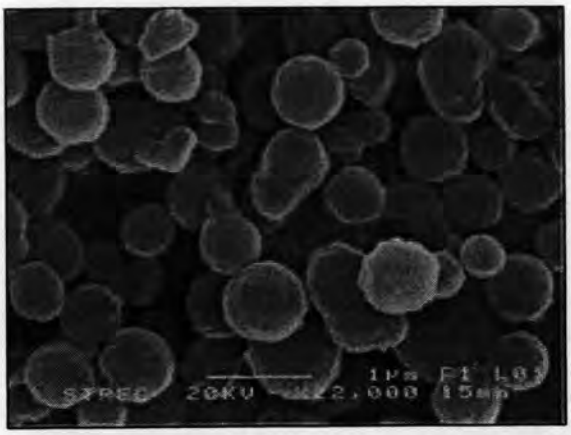

Figure 3.20 SEM photograph at 20 kV of ascorbyl palmitate-loaded-particle **d** (×22,000)

3.1.6 Encapsulation of Astaxanthin into Particle **d**

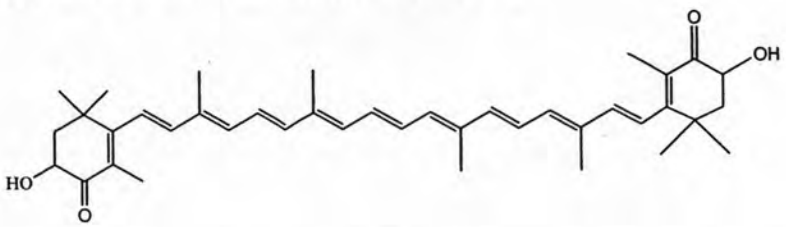

Figure 3.21

Astaxanthin (3, 3'-dihydroxy-β-β'-carotene-4-4'-dione, Figure 3.21) is a natural color carotenoid found in salmon, shrimps, krill and crab. This carotenoid pigment has important applications in the nutraceutical, cosmetic, food and feed industries. Haematococcus pluvialis is the richest source of natural astaxanthin. Astaxanthin is a strong colouring agent, a potent antioxidant, excellent prevention of lipid peroxidation and effective anti-inflammatory [67]. As most carotenoids, astaxanthin is highly unsaturated molecule and thus, can easily be degraded by thermal or oxidative processes during the manufacture and storage of foods [69]. This can cause the loss of their nutritive and biological desirable flavor or aroma compounds. In this work, encapsulation of astaxanthin into nanoparticle by solvent displacement method was carried out.

As can be seen in the TEM photographs (Figure 3.22), the size of the particle increases upon encapsulation. Successful encapsulation of astaxanthin into particle **d** was confirmed through the UV absorption spectra (Figure 3.24). The particles **d** with and without astaxanthin entrapment showed significant difference in UV absorption. It is obvious that an increase absorption at 472 nm of the astaxanthin-loaded-capsules was caused by the presence of astaxanthin. The average sizes of the astaxanthin-

loaded-particle **d** were observed to be 200 nm as determined by SEM (Figure 3.23). With the condition used, about 100% (w/w) astaxanthin could be encapsulated into the particle. The obtained astaxanthin-loaded-capsule contains 38.6% (w/w) astaxanthin (Table 3) (see Appendix A for calculation).

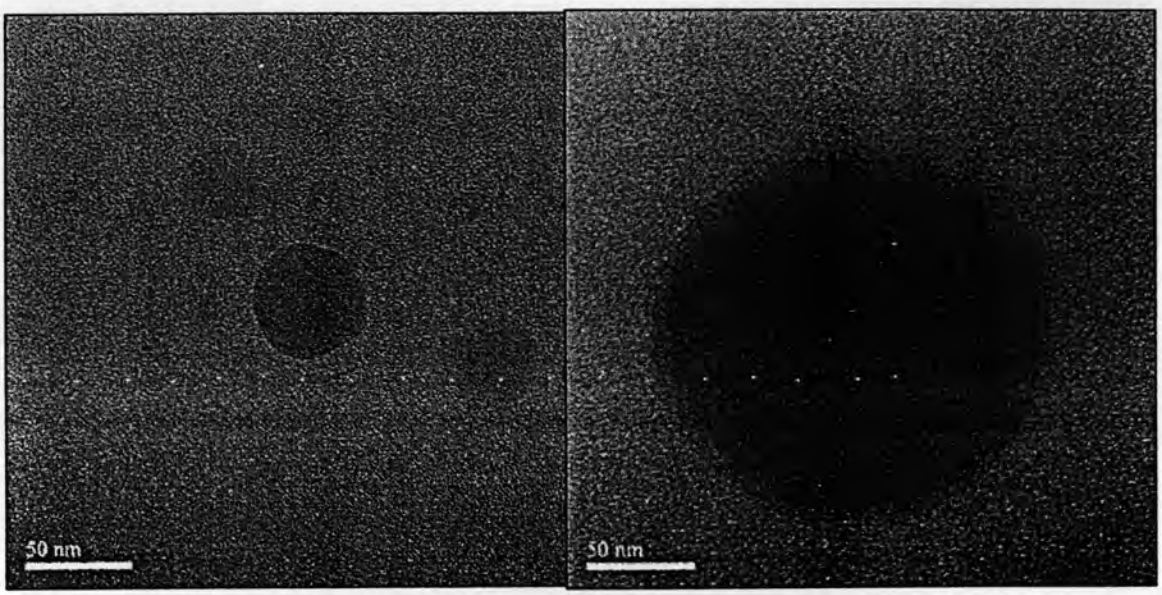

Figure 3.22 TEM images of particle **d** before (left) (×80,000) and after (right) astaxanthin encapsulation (×80,000)

Figure 3.23 SEM photographs at 15 kV of astaxanthin-loaded-particle **d** (×8,500)

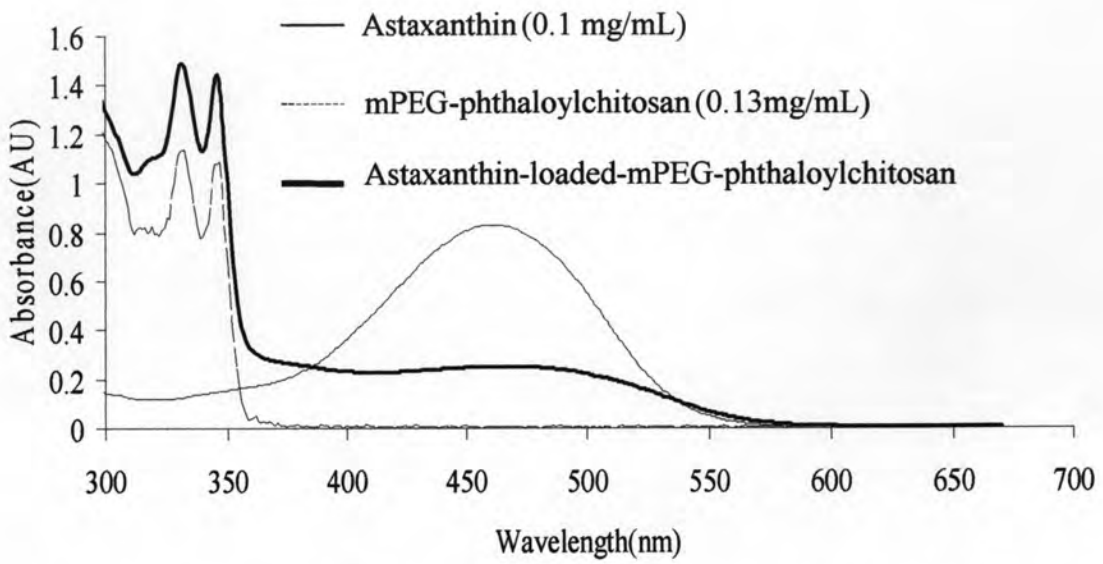

Figure 3.24 UV absorption spectra of astaxanthin-loaded-particle **d** (0.055 mg/ml in DMSO)

Table 3 % Encapsulation efficiency (EE) and % Weight of the active in the particle **d** (%w/w)

Cosmetic actives	EHMC	Astaxanthin	Ascorbyl palmitate
% Encapsulation efficiency*	97.65	100	100
% Weight of the active in the particle **d**** (%w/w)	45	38.6	93.56

*, ** see APPENDIX A for calculation

Figure 3.25 Nanoparticle suspensions from left to right: particle **d**, EHMC-loaded-, ascorbyl palmitate-loaded- and astaxanthin-loaded-particle **d**

3.2 mPEG-4-methoxycinnamoly-phthaloylchitosan Nanoparticles (**e**)

Grafting of 4-methoxycinnamic acid and mPEG-COOH onto *N*-phthaloylchitosan was done successfully using the same method used for grafting of only mPEG-COOH (Scheme 6). The reaction gave 72.4% yield. The brown solid product was characterized by ^{1}H-NMR and IR spectroscopy. Obvious resonances at 8.03-7.93 (Ar-C**H**=CH-), 6.60-6.30 (Ar-CH=C**H**) and 3.73-3.60 (OC**H**$_3$) indicated 4-methoxycinnamoyl moieties. Resonance at 3.91-3.72 ppm indicated mPEG-COOH moieties. IR spectrum peak at 1773 (C=O of ester) and 1618 (C=C) cm^{-1} also helped confirming successful grafting (see Figure 3.27). Since 4-methoxycinnamic acid showed UV absorption at λ_{max} of 310 nm, it was unexpected to see an increase of the UV absorption in the UV absorption spectrum of the grafted product at 330 nm. This bathochromic shift might be a result of some interaction among chromophores on the polymer chain. Comparing with phthaloylchitosan which has absorption band (λ_{max}) at 284, this UV absorption characteristic indicated that 4-methoxycinnamic acid group was successfully grafted onto the chitosan polymer. However, after about 1 day, the absorption of the solution changed to λ_{max} of 300 nm (see Figure 3.29). There was no involvement of light in this shift. The blue shift from 330 to 300 nm was speculated as a complete solvation around 4-methoxycinnamoyl moiety and, therefore, a disruption of interaction among chromophores.

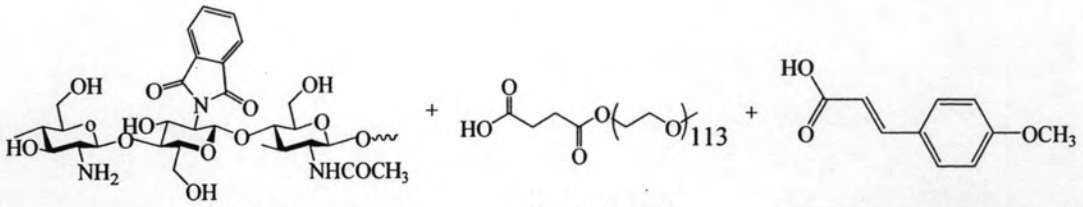

N-phthaloylchitosan
b

mPEG-COOH
c

4- methoxycinnamic acid

EDCI
HOBt

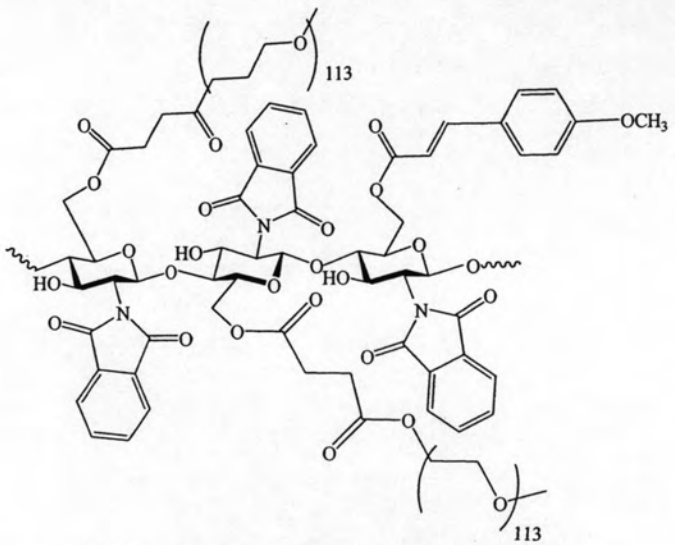

mPEG-4-methoxycinnamoyl-phthaloylchitosan
(compound **e**)

dialysis (solvent displacement process)

mPEG-4-methoxycinnamoyl-phthaloylchitosan
(particle **e**)

Scheme 3.6

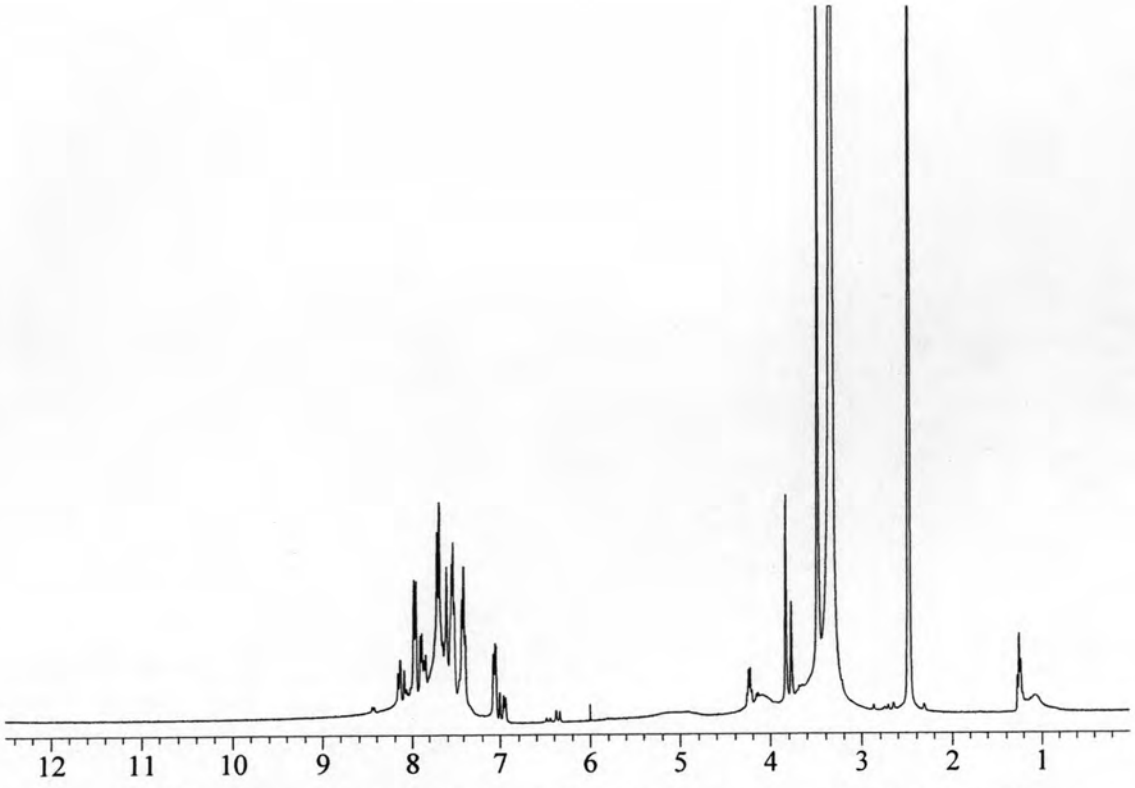

Figure 3.26 ^{1}H-NMR spectrum of mPEG-4-methoxycinnamoyl-phthaloylchitosan (particle **e**) (DMSO deuterated)

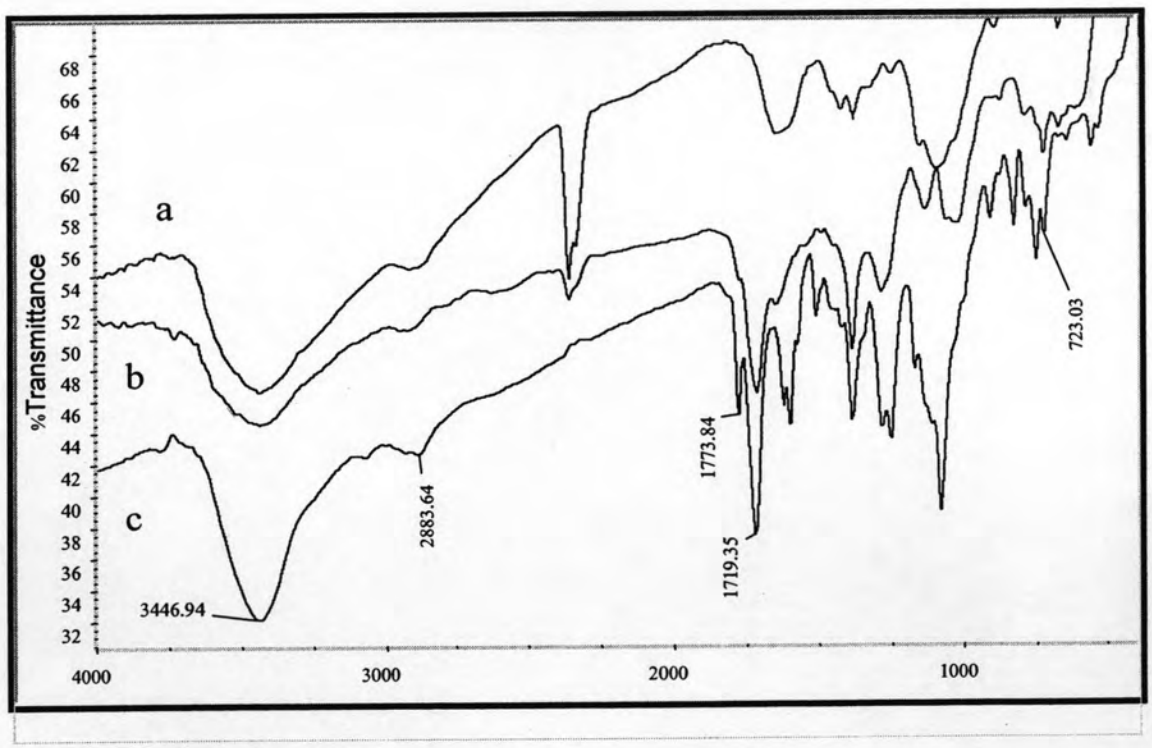

Figure 3.27 IR spectra (KBr) of a) chitosan (compound **a**)

b) *N*-phthaloylchitosan (compound **b**)

c) mPEG-4-methoxycinnamoyl-phthaloylchitosan (particle **e**)

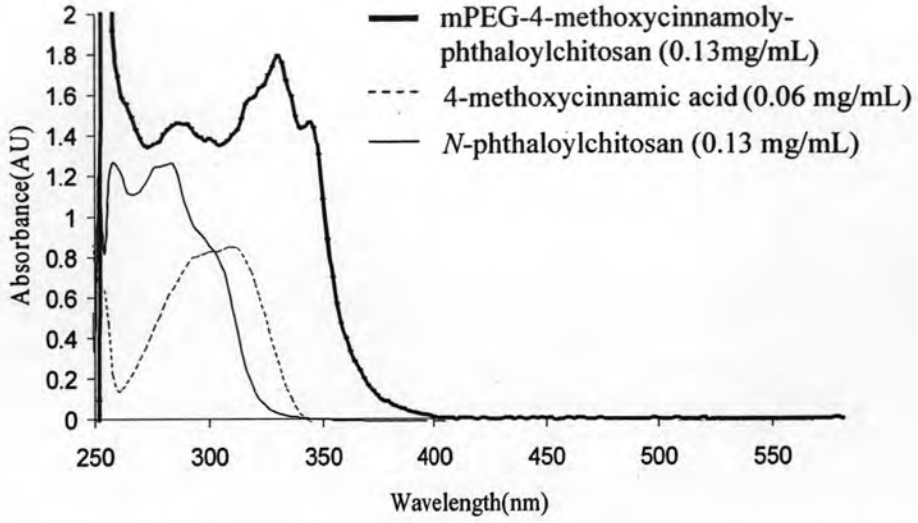

Figure 3.28 UV absorption spectra of mPEG-4-methoxycinnamoyl-phthaloylchitosan (0.13 mg/ml in DMSO)

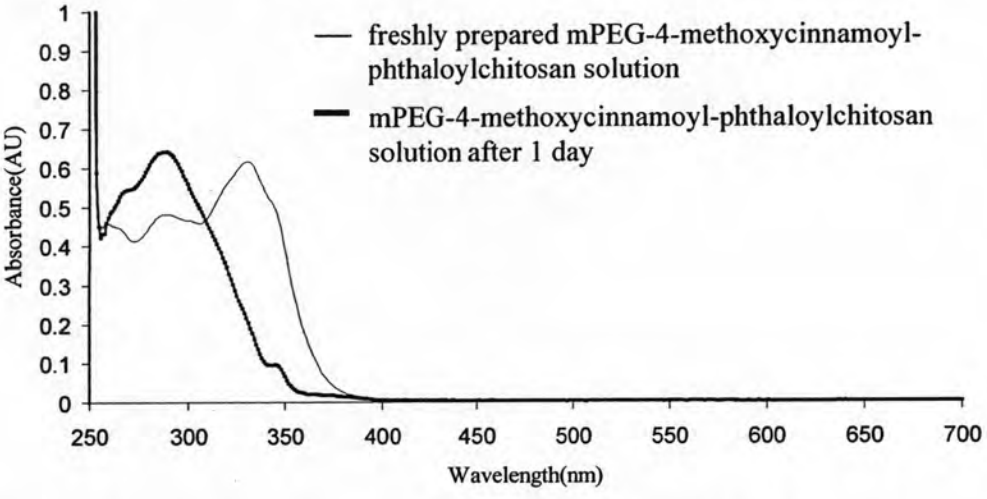

Figure 3.29 UV absorption spectra of freshly prepared mPEG-4-methoxycinnamoyl-phthaloylchitosan (0.05 mg/ml in DMSO)

Substitution percentage of 4-methoxycinnamoyl and PEG moieties on mPEG-4-methoxycinnamoyl-phthaloylchitosan could be obtained from ^{1}H-NMR spectrum. The resonance at 6.3-6.6 ppm represented 1H from Ar-CH=C**H** of the 4-methoxycinnamate. Thus 5 × peak area of 6.3-6.6 ppm gave the total peak area from the other 5H of the 4-methoxycinnamoyl moieties (4H from aromatic ring and 1H from Ph-C**H**=CH). This calculated value was then substrated out from the 6.9-8.6 ppm peak area to obtain the 4H phthaloyl peak area. Thus the ratio between 4-methoxycinnamoyl moiety and phthaloyl moiety could be obtained.

The 3 × peak area of 6.3-6.6 ppm gave the peak area of $-OCH_3$ of the 4-methoxycinnamoyl moiety. This area will be called area a.

From the obtained peak area of phthaloyl moiety, the peak area of the 7 pyranose protons could be estimated. This area will be called area b. Finally the HOD peak area could also be estimated from the ratio obtained as described previously (p.38) using the DMSO peak (2.5 ppm). This area will be called c. As a result, peak area of PEG could be estimated as follow:

Peak area of PEG = Total peak area from 3.0-5.8 ppm - a - b - c

Calculation gave %substitution of 4-methoxycinnamoyl and PEG moieties of 5.70 and 0.313, respectively. General structure of the product is as followed:

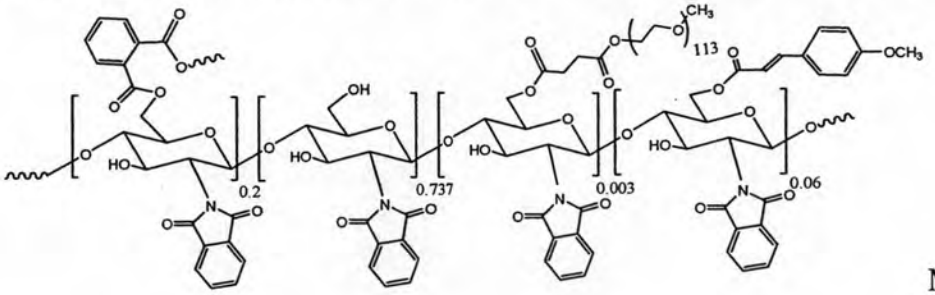

M.W. 218,748

Induction of *N*-phthaloylchitosan into particle **e** by solvent displacement method (displacing DMF with water) gave nanoparticles with diameter ~100-450 nm. SEM photograph at 14 kV of particle **e** is shown in Figure 3.30.

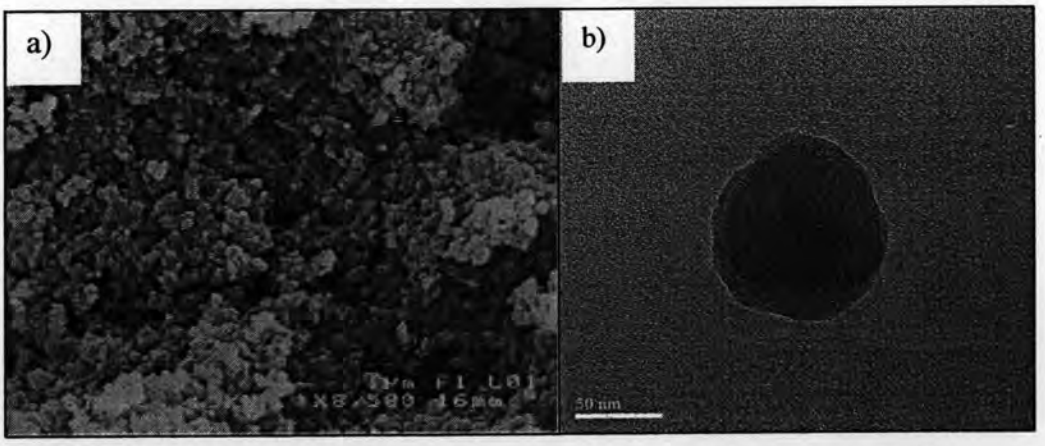

Figure 3.30 a) SEM photographs at 15 kV of mPEG-4-methoxycinnamoyl-phthaloylchitosan nanoparticles (particle **e**) (×8,500)
b) TEM photographs of mPEG-4-methoxycinnamoyl-phthaloylchitosan nanoparticles (particle **e**) (×80,000)

It is important to note that after the mPEG-COOH and 4-methoxycinnamic acid was grafted onto N-phthaloylchitosan; the compound gave a milky solution in water and the turbidity was maintained for a long period of time (~1 months). The milky appearance might be a result of self-aggregation based on the hydrophobic phthalimido groups and aromatic ring of 4-methoxycinnamoyl on the chitosan chain. We speculated that the sphere formation might occur mainly from the aggregation of chitosan chains under the hydrophobic and hydrophilic interaction as shown in scheme 7. From the result of SEM and TEM photograph, the image showed average size 100-450 nm in diameter. The results of the zeta potential indicates a marked negative charge (-31.53 mV) of the mPEG-4-methoxycinnamoyl-phthaloylchitosan. Average particle size distribution of the particles is 295 nm. Anti-microbial study of aqueous mPEG-4-methoxycinnamoyl-phthaloylchitosan dispersion using *Staphylococcus aureus* ATCC 25923 and *Escherichia coli* ATCC 25922 bacteria, indicates that the mPEG-phthaloylchitosan nanoparticles can halt the growth of both bacteria when used at concentration of at least 2500 ppm. The nanoparticles, however, are not bacteriocidal.

Colloidal phenomena and effect of solvent

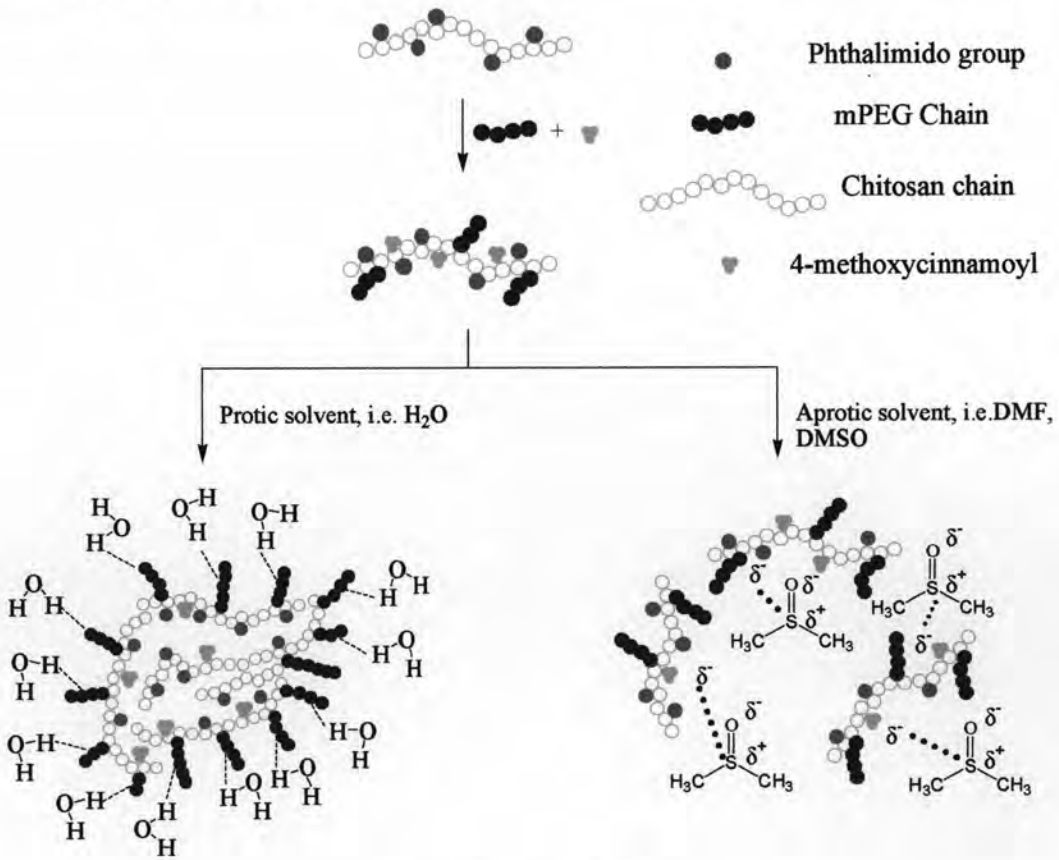

Scheme 3.7

From the study about re-dialysis of particle **e** at concentration 3000 ppm found that it effected aggregation of aqueous particle **e** dispersion. To solve the problem, formulation of aqueous particle **e** dispersion in various stabilizers include gel, tween 1 %, PEG-400 and mPEG 5000 for 3 months was carried out.

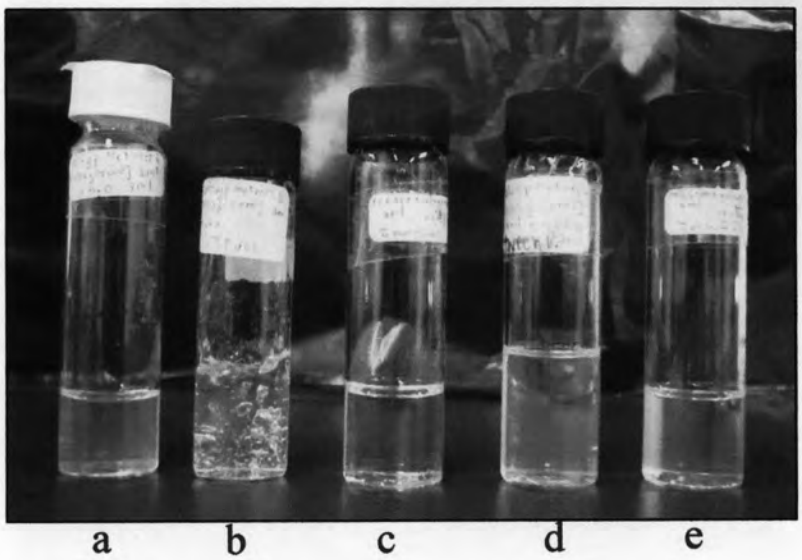

Figure 3.31 Formulation of nanoparticles **e** in various stabilizers at room temperature a) no stabilizer (b) gel (c) PEG-400 (d) tween 1% (e) mPEG 5000 [freshly prepared]

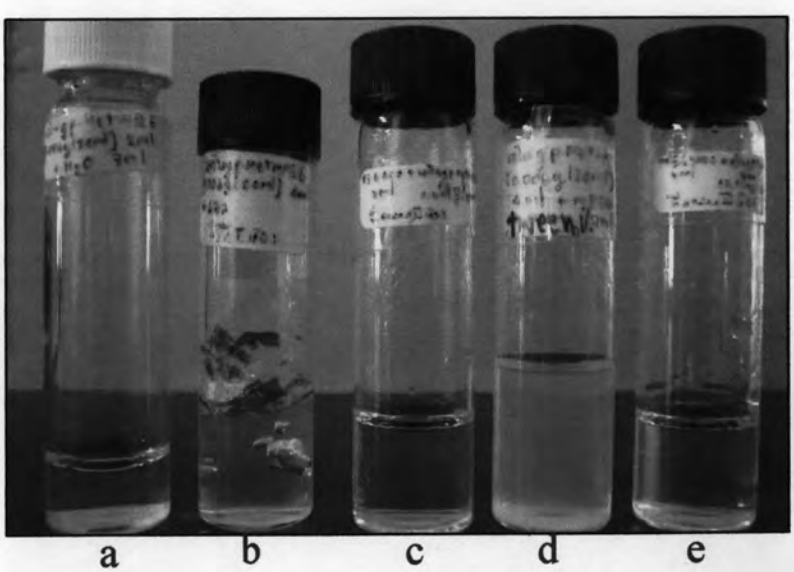

Figure 3.32 Formulation of nanoparticles **e** in various stabilizers at room temperature a) no stabilizer (b) gel (c) PEG-400 (d) tween 1% (e) mPEG 5000 [after 3 month]

As mentioned above, the results demonstrated that the aqueous particle **e** could well disperse in mPEG 5000 and PEG 400, whereas formulation in gel and tween 1% showed aggregation of aqueous nanoparticle **e**. Moreover, formulation of aqueous nanoparticles **e** in mPEG 5000 and PEG-400 could also well disperse at 4°C and 50°C after 3 month.

After successful preparation and characterization of particle **e**, various cosmetic actives are being encapsulated into the prepared particles.

3.2.1 Encapsulation of Ascorbyl Palmitate into Particle **e**

Encapsulation was done through 1) solvent displacement technique in which the ascorbyl palmitate and chitosan were dissolved in DMF and then DMF was then displaced by water and 2) diffusion method in which ascorbyl palmitate was added into aqueous suspension of nanoparticle **e** and stirring was maintained over a period of time to allow diffusion of ascorbyl palmitate into the particle.

In the solvent displacement method, study was carried out to investigate the effects of encapsulation of ascorbyl palmitate into nanoparticles **e** on encapsulation efficiency (EE).

Since ascorbyl palmitate has no obvious well seperated UV-visible absorption band when compared to UV absorption spectrum of particle **e**, NMR spectroscopy was used for the analyses of ascorbyl palmitate loaded particle **e.** After encapsulation process, the washed particle were dissolved in DMSO and subjected to NMR analyses. Presences of ^{1}H resonances at 0.8 and 1.4 ppm (representing palmitoyl moieties in ascorbyl palmitate, Figure 3.33) confirm a successful encapsulation of this vitamin C derivative into particle **e.** TEM photographs (Figure 3.34), after ascorbyl palmitate encapsulation the appearance of particle's border is very apparent. Encapsulation shows obvious size changes. The average sizes of the ascorbyl palmitate-loaded-nanoparticle were observed to be ~200-650 nm (diameter) as determined by SEM (Figure 3.35). The encapsulated particles appeared well dispersed in water (Figure 3.39). With the condition used, about 100% (w/w) ascorbyl palmitate could be encapsulated into the particle **e**. The obtained ascorbyl palmitate-loaded-capsule contains 68.88% (w/w) ascorbyl palmitate (Table 4) (see in Appendix A for calculation).

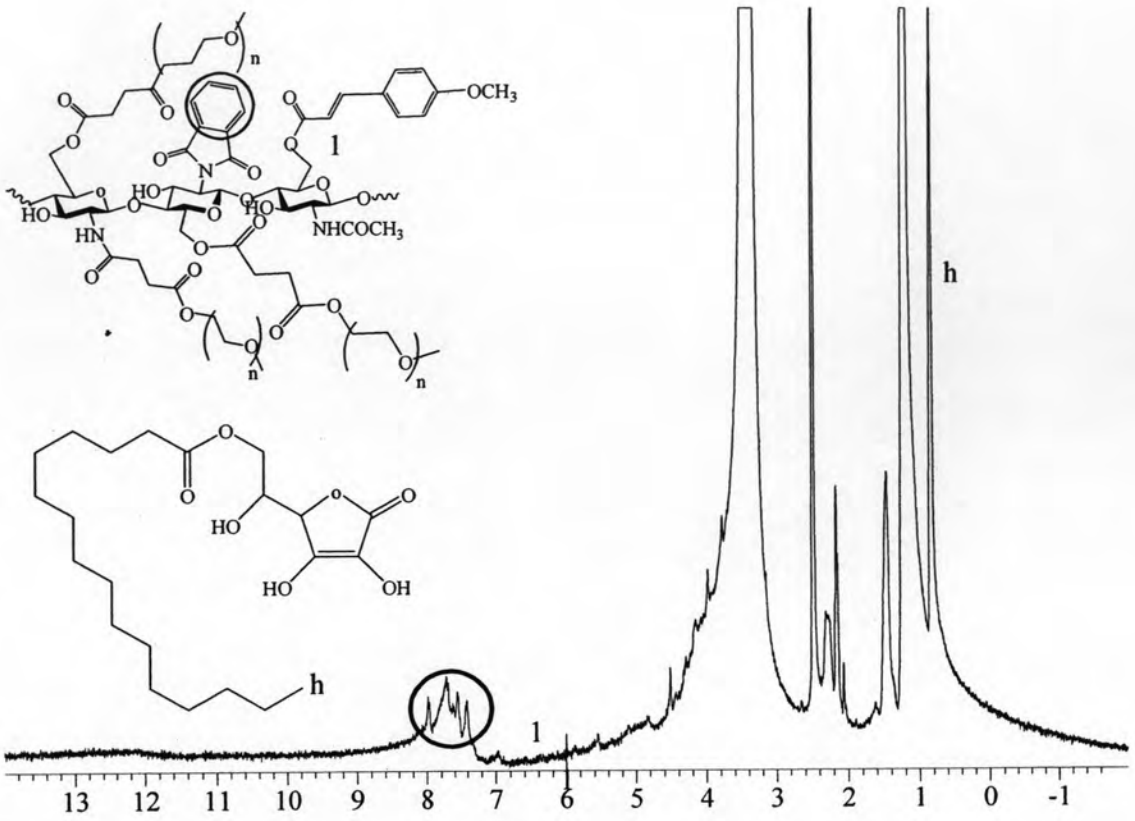

Figure 3.33 ^{1}H-NMR spectrum of ascorbyl palmitate-loaded-particle **e** (0.0061 g of deuterated DMSO)

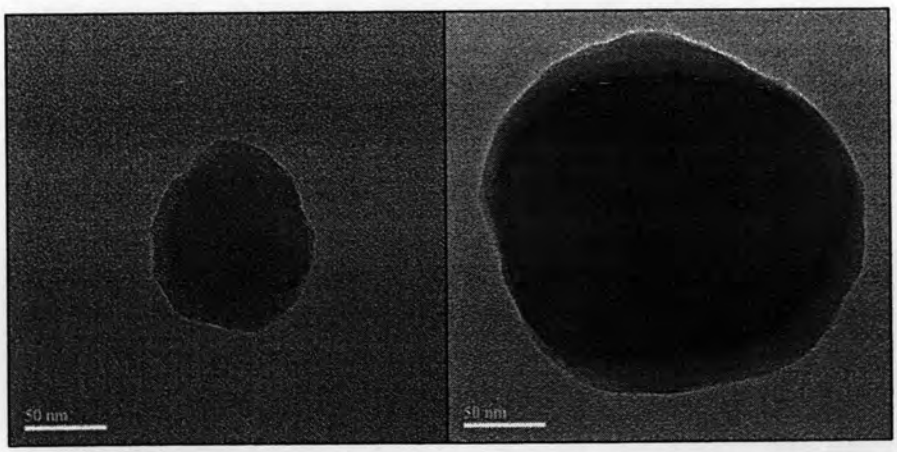

Figure 3.34 TEM photographs of particle **e** before (left) (×80,000) and after (right) ascorbyl palmitate encapsulation (×80,000)

Figure 3.35 SEM photograph at 20 kV of ascorbyl palmitate-loaded-particle **e** (×22,000)

Moreover, the diffusion method was also carried out to investigate the effects of diffusion of ascorbyl palmitate into particle **e** on diffusion efficiency. The results indicated that the active was increasingly loaded into nanoparticle **e** when spend any more time. This was judged from NMR absorption spectrum of the obtained particles. ^{1}H-NMR resonance at 1.4 ppm represents palmitoyl moieties in ascorbyl palmitate.

Table 4 % Diffusion efficiency and % Weight of ascorbyl palmitate in the particle **e** (%w/w)

Process	Time				
	0 second	5 day	10 day	20 day	30 day
% Weight of ascorbyl palmitate into the particle **e** (%w/w)*	73.93	84.15	94.44	94.44	94.44
% Diffusion efficiency**	98.51	100	100	100	100

*, ** see APPENDIX A for calculation

The results indicated that diffusion method gave better efficiency of diffusion of ascorbyl palmitate into particle **e** than which solvent displacement method.

3.2.2 Encapsulation of Astaxanthin into Particle **e**

As can be seen in the TEM photographs (Figure 3.36), after astaxanthin encapsulation, the appearance of particle's border is very apparent. The size of the particle also increases upon encapsulation. Successful encapsulation of astaxanthin into particle **e** was confirmed through the UV absorption spectra (Figure 3.38). The particle **e** with and without astaxanthin entrapment showed significant difference

in UV absorption. It is obvious that an increase absorption at 492 nm of the astaxanthin-loaded-capsules was caused by the presence of astaxanthin. The average sizes of the astaxanthin-loaded-particle **e** were observed to be ~250-550 nm as determined by SEM (Figure 3.37). With the condition used, about 100% (w/w) astaxanthin could be encapsulated into the particle. The obtained astaxanthin-loaded-capsule contains 22.13% (w/w) astaxanthin (Table 5) (see Appendix A).

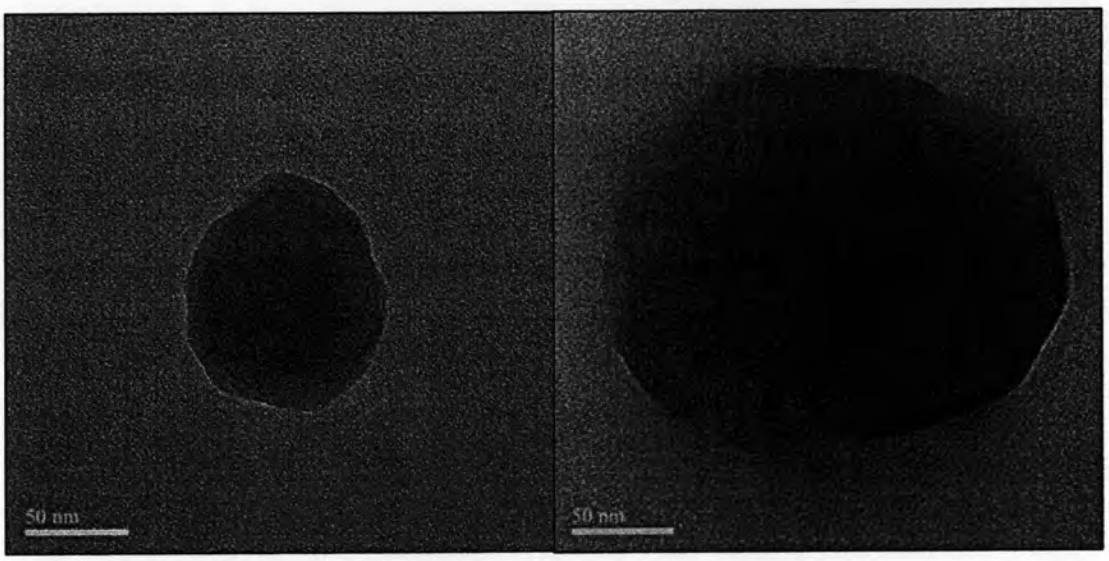

Figure 3.36 TEM photographs of particle **e** before (left) (×80,000) and after (right) astaxanthin encapsulation (×80,000)

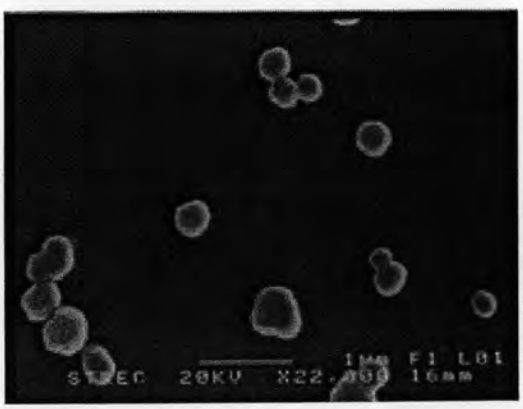

Figure 3.37 SEM photographs at 15 kV of astaxanthin-loaded-particle **e** (×8,500)

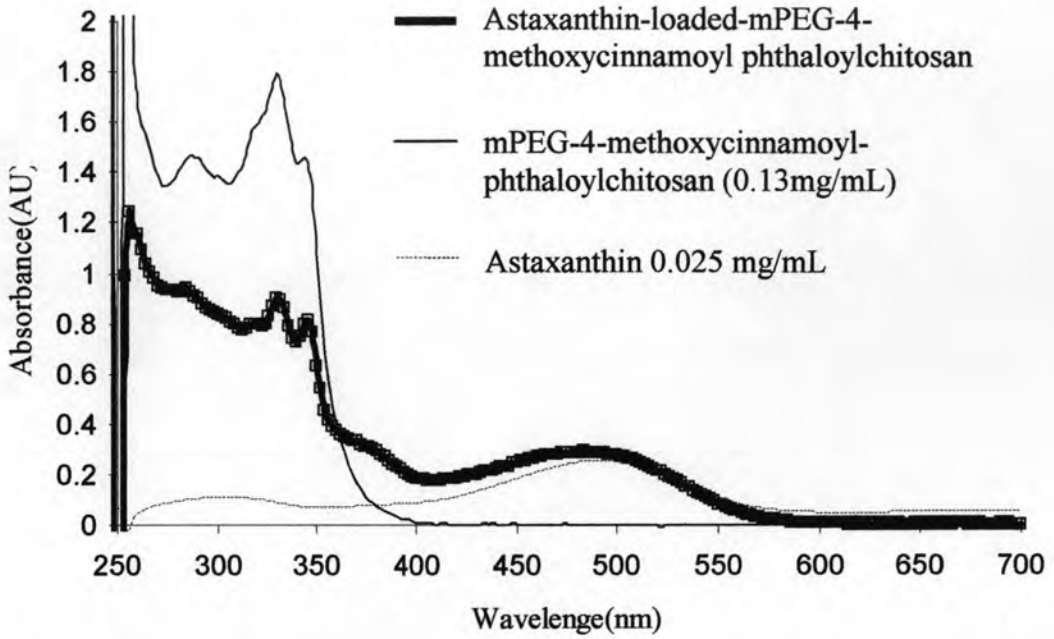

Figure 3.38 UV absorption spectra of mPEG-4-methoxycinnamoyl-phthaloylchitosan nanoparticles (particle **e**) (0.11 mg/ mL in DMSO)

Table 5 % Encapsulation efficiency (EE) and %Weight of the active in the particle **e** (%w/w)

Cosmetic actives	Astaxanthin	Ascorbyl palmitate
% Encapsulation efficiency*	100	100
%Weight of the active in the particle **e**** (% w/w)	22.13	68.88

*, ** see APPENDIX A for calculation

Figure 3.39 Nanoparticle suspensions from left to right: particle **e**, ascorbyl palmitate-loaded- and astaxanthin-loaded-particle **e**